Searching for Solar KDAR with DUNE

The DUNE Collaboration

A. Abed Abud[125,25] B. Abi[151] R. Acciarri[65] M. A. Acero[11]
M. R. Adames[187] G. Adamov[70] D. Adams[21] M. Adinolfi[20]
A. Aduszkiewicz[79] J. Aguilar[124] Z. Ahmad[199] J. Ahmed[202]
B. Ali-Mohammadzadeh[85,37] T. Alion[185] K. Allison[44] S. Alonso
Monsalve[25,57] M. Alrashed[118] C. Alt[57] A. Alton[12] P. Amedo[83]
J. Anderson[7] C. Andreopoulos[171,125] M. Andreotti[86,66]
M. P. Andrews[65] F. Andrianala[5] S. Andringa[122] N. Anfimov[110]
A. Ankowski[172] M. Antoniassi[187] M. Antonova[82] A. Antoshkin[110]
S. Antusch[14] A. Aranda-Fernandez[43] A. Ariga[15] L. O. Arnold[46]
M. A. Arroyave[56] J. Asaadi[190] L. Asquith[185] A. Aurisano[41]
V. Aushev[121] D. Autiero[96] M. Ayala-Torres[42] F. Azfar[151] A. Back[104]
H. Back[152] J. J. Back[202] C. Backhouse[196] P. Baesso[20] I. Bagaturia[70]
L. Bagby[65] N. Balashov[110] S. Balasubramanian[65] P. Baldi[30]
B. Baller[65] B. Bambah[80] F. Barao[122,98] G. Barenboim[82]
G. J. Barker[202] W. Barkhouse[144] C. Barnes[134] G. Barr[151]
J. Barranco Monarca[75] A. Barros[187] N. Barros[122,59] J. L. Barrow[131]
A. Basharina-Freshville[196] A. Bashyal[150] V. Basque[130] E. Belchior[36]
J.B.R. Battat[203] F. Battisti[151] F. Bay[4] J. L. Bazo Alba[163]
J. F. Beacom[149] E. Bechetoille[96] B. Behera[45] L. Bellantoni[65]
G. Bellettini[161] V. Bellini[85,37] O. Beltramello[25] D. Belver[26]
N. Benekos[25] C. Benitez Montiel[9] F. Bento Neves[122] J. Berger[45]
S. Berkman[65] P. Bernardini[88,174] R. M. Berner[15] H. Berns[29]
S. Bertolucci[84,18] M. Betancourt[65] A. Betancur Rodríguez[56]
A. Bevan[166] T.J.C. Bezerra[185] V. Bhatnagar[154] M. Bhattacharjee[102]
S. Bhuller[20] B. Bhuyan[102] S. Biagi[94] J. Bian[30] M. Biassoni[89]
K. Biery[65] B. Bilki[16,107] M. Bishai[21] A. Bitadze[130] A. Blake[123]
F. D. M. Blaszczyk[65] G. C. Blazey[145] E. Blucher[39] J. Boissevain[126]
S. Bolognesi[24] T. Bolton[118] L. Bomben[89,106] M. Bonesini[89,136]
M. Bongrand[155] F. Bonini[21] A. Booth[166] C. Booth[177] F. Boran[16]
S. Bordoni[25] A. Borkum[185] T. Boschi[55] N. Bostan[107,147] P. Bour[48]

C. Bourgeois[155] S. B. Boyd[202] D. Boyden[145] J. Bracinik[17]
D. Braga[65] D. Brailsford[123] A. Branca[89] A. Brandt[190] J. Bremer[25]
C. Brew[171] E. Brianne[130] S. J. Brice[65] C. Brizzolari[89,136]
C. Bromberg[135] G. Brooijmans[46] J. Brooke[20] A. Bross[65]
G. Brunetti[89,136] M. Brunetti[202] N. Buchanan[45] H. Budd[168]
I. Butorov[110] I. Cagnoli[84,18] D. Caiulo[96] R. Calabrese[86,66]
P. Calafiura[124] J. Calcutt[135] M. Calin[22] S. Calvez[45] E. Calvo[26]
A. Caminata[87] M. Campanelli[196] K. Cankocak[107] D. Caratelli[65]
G. Carini[21] B. Carlus[96] M. F. Carneiro[21] P. Carniti[89] I. Caro
Terrazas[45] H. Carranza[190] T. Carroll[206] J. F. Castaño Forero[6]
A. Castillo[176] C. Castromonte[105] E. Catano-Mur[205] C. Cattadori[89]
F. Cavalier[155] F. Cavanna[65] S. Centro[153] G. Cerati[65] A. Cervelli[84]
A. Cervera Villanueva[82] M. Chalifour[25] A. Chappell[202]
E. Chardonnet[156] N. Charitonidis[25] A. Chatterjee[162]
S. Chattopadhyay[199] H. Chen[21] M. Chen[30] Y. Chen[15] Z. Chen[182]
Y. Cheon[194] D. Cherdack[79] C. Chi[46] S. Childress[65] A. Chiriacescu[22]
G. Chisnall[185] K. Cho[116] S. Choate[145] D. Chokheli[70] P. S. Chong[158]
S. Choubey[76] A. Christensen[45] D. Christian[65] G. Christodoulou[25]
A. Chukanov[110] M. Chung[194] E. Church[152] V. Cicero[84,18] P. Clarke[58]
T. E. Coan[181] A. G. Cocco[91] J. A. B. Coelho[156] E. Conley[54]
R. Conley[172] J. M. Conrad[131] M. Convery[172] S. Copello[87]
L. Corwin[178] R. Valentim[195] L. Cremaldi[140] L. Cremonesi[166]
J. I. Crespo-Anadón[26] M. Crisler[65] E. Cristaldo[9] R. Cross[123]
A. Cudd[44] C. Cuesta[26] Y. Cui[32] D. Cussans[20] O. Dalager[30] H. da
Motta[23] L. Da Silva Peres[64] C. David[209,65] Q. David[96]
G. S. Davies[140] S. Davini[87] J. Dawson[156] K. De[190] P. Debbins[107]
I. De Bonis[51] M. P. Decowski[143,3] A. de Gouvêa[146] P. C. De
Holanda[36] I. L. De Icaza Astiz[185] A. Deisting[169] P. De Jong[143,3]
A. Delbart[24] D. Delepine[75] M. Delgado[6] A. Dell'Acqua[25] P. De
Lurgio[7] J. R. T. de Mello Neto[64] D. M. DeMuth[198] S. Dennis[35]
C. Densham[171] G. W. Deptuch[21] A. De Roeck[25] V. De Romeri[82]
G. De Souza[36] R. Devi[111] R. Dharmapalan[78] M. Dias[195] F. Diaz[163]
J. S. Díaz[104] S. Di Domizio[87,69] L. Di Giulio[25] P. Ding[65] L. Di
Noto[87,69] C. Distefano[94] R. Diurba[139] M. Diwan[21] Z. Djurcic[7]
D. Doering[172] S. Dolan[25] F. Dolek[16] M. J. Dolinski[53] L. Domine[172]
D. Douglas[135] D. Douillet[155] G. Drake[65] F. Drielsma[172] L. Duarte[195]
D. Duchesneau[51] K. Duffy[65] P. Dunne[101] T. Durkin[171] H. Duyang[180]
O. Dvornikov[78] D. A. Dwyer[124] A. S. Dyshkant[145] M. Eads[145]
A. Earle[185] D. Edmunds[135] J. Eisch[65] L. Emberger[130,132] S. Emery[24]

A. Ereditato[207] T. Erjavec[29] C. O. Escobar[65] G. Eurin[24]
J. J. Evans[130] E. Ewart[104] A. C. Ezeribe[177] K. Fahey[65]
A. Falcone[89,136] M. Fani'[126] C. Farnese[92] Y. Farzan[97] D. Fedoseev[110]
J. Felix[75] Y. Feng[108] E. Fernandez-Martinez[129] P. Fernandez
Menendez[82] M. Fernandez Morales[83] F. Ferraro[87,69] L. Fields[147]
P. Filip[47] F. Filthaut[143,167] A. Fiorentini[178] M. Fiorini[86,66]
R. S. Fitzpatrick[134] W. Flanagan[50] B. Fleming[207] R. Flight[168]
D. V. Forero[133] J. Fowler[54] W. Fox[104] J. Franc[48] K. Francis[145]
D. Franco[207] J. Freeman[65] J. Freestone[130] J. Fried[21] A. Friedland[172]
F. Fuentes Robayo[20] S. Fuess[65] I. K. Furic[67] A. P. Furmanski[139]
A. Gabrielli[84] A. Gago[163] H. Gallagher[193] A. Gallas[155]
A. Gallego-Ros[26] N. Gallice[90,137] V. Galymov[96] E. Gamberini[25]
T. Gamble[177] F. Ganacim[187] R. Gandhi[76] R. Gandrajula[135] F. Gao[162]
S. Gao[21] A. C. Garcia B.[36] D. Garcia-Gamez[73] M. Á. García-Peris[82]
S. Gardiner[65] D. Gastler[19] J. Gauvreau[148] G. Ge[46] B. Gelli[36]
A. Gendotti[57] S. Gent[179] Z. Ghorbani-Moghaddam[87]
P. Giammaria[36] T. Giammaria[86,66] D. Gibin[153] I. Gil-Botella[26]
S. Gilligan[150] C. Girerd[96] A. K. Giri[103] D. Gnani[124] O. Gogota[121]
M. Gold[141] S. Gollapinni[126] K. Gollwitzer[65] R. A. Gomes[61]
L. V. Gomez Bermeo[176] L. S. Gomez Fajardo[176] F. Gonnella[17]
J. A. Gonzalez-Cuevas[9] D. Gonzalez Diaz[83] M. Gonzalez-Lopez[129]
M. C. Goodman[7] O. Goodwin[130] S. Goswami[160] C. Gotti[89]
E. Goudzovski[17] C. Grace[124] M. Graham[172] R. Gran[138]
E. Granados[75] P. Granger[24] A. Grant[52] C. Grant[19] D. Gratieri[68]
P. Green[130] L. Greenler[206] J. Greer[20] J. Grenard[25] W. C. Griffith[185]
M. Groh[45] J. Grudzinski[7] K. Grzelak[201] W. Gu[21] E. Guardincerri[126]
V. Guarino[7] M. Guarise[86,66] R. Guenette[77] E. Guerard[155]
M. Guerzoni[84] A. Guglielmi[92] B. Guo[180] K. K. Guthikonda[117]
R. Gutierrez[6] P. Guzowski[130] M. M. Guzzo[36] S. Gwon[40] C. Ha[40]
A. Habig[138] H. Hadavand[190] R. Haenni[15] A. Hahn[65] J. Haiston[178]
P. Hamacher-Baumann[151] T. Hamernik[65] P. Hamilton[101] J. Han[162]
D. A. Harris[209,65] J. Hartnell[185] J. Harton[45] T. Hasegawa[115]
C. Hasnip[151] R. Hatcher[65] K. W. Hatfield[30] A. Hatzikoutelis[175]
C. Hayes[104] K. Hayrapetyan[166] J. Hays[166] E. Hazen[19] M. He[79]
A. Heavey[65] K. M. Heeger[207] J. Heise[173] K. Hennessy[125]
S. Henry[168] M. A. Hernandez Morquecho[100] K. Herner[65]
L. Hertel[30] J. Hewes[41] A. Higuera[79] T. Hill[99] S. J. Hillier[17]
A. Himmel[65] L.R. Hirsch[187] J. Ho[77] J. Hoff[65] A. Holin[171]
E. Hoppe[152] G. A. Horton-Smith[118] M. Hostert[139] A. Hourlier[131]

B. Howard[65] R. Howell[168] I. Hristova[171] M. S. Hronek[65] J. Huang[191]
J. Huang[29] J. Hugon[127] G. Iles[101] N. Ilic[192] A. M. Iliescu[84]
R. Illingworth[65] G. Ingratta[84,18] A. Ioannisian[208] L. Isenhower[1]
R. Itay[172] A. Izmaylov[82] C.M. Jackson[152] V. Jain[2] E. James[65]
W. Jang[190] B. Jargowsky[30] F. Jediny[48] D. Jena[65] Y. S. Jeong[40,107]
C. Jesús-Valls[81] X. Ji[21] L. Jiang[200] S. Jiménez[26] A. Jipa[22]
R. Johnson[41] N. Johnston[104] B. Jones[190] S. B. Jones[196]
M. Judah[162] C. K. Jung[182] T. Junk[65] Y. Jwa[46] M. Kabirnezhad[151]
A. Kaboth[169,171] I. Kadenko[121] D. Kaira[46] I. Kakorin[110]
A. Kalitkina[110] F. Kamiya[63] N. Kaneshige[33] G. Karagiorgi[46]
G. Karaman[107] A. Karcher[124] M. Karolak[24] Y. Karyotakis[51]
S. Kasai[120] S. P. Kasetti[127] L. Kashur[45] N. Kazaryan[208] E. Kearns[19]
P. Keener[158] K.J. Kelly[65] E. Kemp[36] O. Kemularia[70] W. Ketchum[65]
S. H. Kettell[21] M. Khabibullin[95] A. Khotjantsev[95] A. Khvedelidze[70]
D. Kim[188] B. King[65] B. Kirby[46] M. Kirby[65] J. Klein[158] K. Koehler[206]
L. W. Koerner[79] S. Kohn[28,124] P. P. Koller[15] L. Kolupaeva[110]
D. Korablev[110] M. Kordosky[205] T. Kosc[96] U. Kose[25]
V. A. Kostelecký[104] K. Kothekar[20] F. Krennrich[108] I. Kreslo[15]
W. Kropp[30] Y. Kudenko[95] V. A. Kudryavtsev[177] S. Kulagin[95]
J. Kumar[78] P. Kumar[177] P. Kunze[51] C. Kuruppu[180] V. Kus[48]
T. Kutter[127] J. Kvasnicka[47] D. Kwak[194] A. Lambert[124] B. J. Land[158]
K. Lande[158] C. E. Lane[53] K. Lang[191] T. Langford[207] M. Langstaff[130]
J. Larkin[21] P. Lasorak[185] D. Last[158] C. Lastoria[26] A. Laundrie[206]
G. Laurenti[84] A. Lawrence[124] I. Lazanu[22] R. LaZur[45]
M. Lazzaroni[90,137] T. Le[193] S. Leardini[83] J. Learned[78] P. LeBrun[96]
T. LeCompte[7] C. Lee[65] S. Y. Lee[113] G. Lehmann Miotto[25]
R. Lehnert[104] M. A. Leigui de Oliveira[63] M. Leitner[124]
L. M. Lepin[130] L. Li[30] S. W. Li[172] T. Li[58] Y. Li[21] H. Liao[118]
C. S. Lin[124] Q. Lin[172] S. Lin[127] J. Ling[184] A. Lister[206]
B. R. Littlejohn[100] J. Liu[30] S. Lockwitz[65] T. Loew[124] M. Lokajicek[47]
I. Lomidze[70] K. Long[101] K. Loo[114] T. Lord[202] J. M. LoSecco[147]
W. C. Louis[126] X.-G. Lu[151] K.B. Luk[28,124] X. Luo[33] E. Luppi[86,66]
N. Lurkin[17] T. Lux[81] V. P. Luzio[63] D. MacFarlane[172]
A. A. Machado[36] P. Machado[65] C. T. Macias[104] J. R. Macier[65]
A. Maddalena[72] A. Madera[25] P. Madigan[28,124] S. Magill[7]
K. Mahn[135] A. Maio[122,59] A. Major[54] J. A. Maloney[49] G. Mandrioli[84]
R. C. Mandujano[30] J. Maneira[122,59] L. Manenti[196] S. Manly[168]
A. Mann[193] K. Manolopoulos[171] M. Manrique Plata[104]
V. N. Manyam[21] L. Manzanillas[155] M. Marchan[65] A. Marchionni[65]

W. Marciano[21] D. Marfatia[78] C. Mariani[200] J. Maricic[78] R. Marie[155]
F. Marinho[62] A. D. Marino[44] D. Marsden[130] M. Marshak[139]
C. M. Marshall[168] J. Marshall[202] J. Marteau[96] J. Martin-Albo[82]
N. Martinez[118] D.A. Martinez Caicedo [178] S. Martynenko[182]
V. Mascagna[89,106] K. Mason[193] A. Mastbaum[170] M. Masud[82]
F. Matichard[124] S. Matsuno[78] J. Matthews[127] C. Mauger[158]
N. Mauri[84,18] K. Mavrokoridis[125] I. Mawby[202] R. Mazza[89]
A. Mazzacane[65] E. Mazzucato[24] T. McAskill[203] E. McCluskey[65]
N. McConkey[130] K. S. McFarland[168] C. McGrew[182] A. McNab[130]
A. Mefodiev[95] P. Mehta[112] P. Melas[10] O. Mena[82] S. Menary[209]
H. Mendez[164] P. Mendez[25] D. P. M[21] A. Menegolli[93,157] G. Meng[92]
M. D. Messier[104] W. Metcalf[127] T. Mettler[15] M. Mewes[104]
H. Meyer[204] T. Miao[65] G. Michna[179] T. Miedema[143,167] V. Mikola[196]
R. Milincic[78] G. Miller[130] W. Miller[139] J. Mills[193] C. Milne[99]
O. Mineev[95] O. G. Miranda[42] S. Miryala[21] C. S. Mishra[65]
S. R. Mishra[180] A. Mislivec[139] D. Mladenov[25] I. Mocioiu[159]
K. Moffat[55] N. Moggi[84,18] R. Mohanta[80] T. A. Mohayai[65]
N. Mokhov[65] J. Molina[9] L. Molina Bueno[82] E. Montagna[84,18]
A. Montanari[84] C. Montanari[93,65,157] D. Montanari[65] L. M. Montano
Zetina[42] J. Moon[131] S. H. Moon[194] M. Mooney[45] A. F. Moor[35]
D. Moreno[6] C. Morris[79] C. Mossey[65] E. Motuk[196] C. A. Moura[63]
J. Mousseau[134] G. Mouster[123] W. Mu[65] L. Mualem[34] J. Mueller[45]
M. Muether[204] S. Mufson[104] F. Muheim[58] A. Muir[52] M. Mulhearn[29]
D. Munford[79] H. Muramatsu[139] S. Murphy[57] J. Musser[104]
J. Nachtman[107] S. Nagu[128] M. Nalbandyan[208] R. Nandakumar[171]
D. Naples[162] S. Narita[109] A. Nath[102] D. Navas-Nicolás[26]
A. Navrer-Agasson[130] N. Nayak[30] M. Nebot-Guinot[58] K. Negishi[109]
J. K. Nelson[205] J. Nesbit[206] M. Nessi[25] D. Newbold[171]
M. Newcomer[158] D. Newhart[65] H. Newton[52] R. Nichol[196]
F. Nicolas-Arnaldos[73] E. Niner[65] K. Nishimura[78] A. Norman[65]
A. Norrick[65] R. Northrop[39] P. Novella[82] J. A. Nowak[123]
M. Oberling[7] J. P. Ochoa-Ricoux[30] A. Olivares Del Campo[55]
A. Olivier[168] A. Olshevskiy[110] Y. Onel[107] Y. Onishchuk[121] J. Ott[30]
L. Pagani[29] S. Pakvasa[78] G. Palacio[56] O. Palamara[65] S. Palestini[25]
J. M. Paley[65] M. Pallavicini[87,69] C. Palomares[26]
J. L. Palomino-Gallo[182] W. Panduro Vazquez[169] E. Pantic[29]
V. Paolone[162] V. Papadimitriou[65] R. Papaleo[94] A. Papanestis[171]
S. Paramesvaran[20] S. Parke[65] E. Parozzi[89,136] Z. Parsa[21] M. Parvu[22]
S. Pascoli[55,18] L. Pasqualini[84,18] J. Pasternak[101] J. Pater[130]

C. Patrick[196] L. Patrizii[84] R. B. Patterson[34] S. J. Patton[124]
T. Patzak[156] A. Paudel[118] B. Paulos[206] L. Paulucci[63] Z. Pavlovic[65]
G. Pawloski[139] D. Payne[125] V. Pec[177] S. J. M. Peeters[185]
E. Pennacchio[96] A. Penzo[107] O. L. G. Peres[36] J. Perry[58]
D. Pershey[54] G. Pessina[89] G. Petrillo[172] C. Petta[85,37] R. Petti[180]
F. Piastra[15] L. Pickering[135] F. Pietropaolo[25,92] R. Plunkett[65]
R. Poling[139] X. Pons[25] N. Poonthottathil[108] F. Poppi[84,18]
S. Pordes[65] J. Porter[185] M. Potekhin[21] R. Potenza[85,37]
B. V. K. S. Potukuchi[111] J. Pozimski[101] M. Pozzato[84,18]
S. Prakash[36] T. Prakash[124] M. Prest[89] S. Prince[77] F. Psihas[65]
D. Pugnere[96] X. Qian[21] M. C. Queiroga Bazetto[36] J. L. Raaf[65]
V. Radeka[21] J. Rademacker[20] B. Radics[57] A. Rafique[7] E. Raguzin[21]
M. Rai[202] M. Rajaoalisoa[41] I. Rakhno[65] A. Rakotonandrasana[5]
L. Rakotondravohitra[5] Y. A. Ramachers[202] R. Rameika[65]
M. A. Ramirez Delgado[158] B. Ramson[65] A. Rappoldi[93,157]
G. Raselli[93,157] P. Ratoff[123] S. Raut[182] R. F. Razakamiandra[5]
E. Rea[139] J.S. Real[74] B. Rebel[206,65] M. Reggiani-Guzzo[130]
T. Rehak[53] J. Reichenbacher[178] S. D. Reitzner[65] H. Rejeb Sfar[25]
A. Renshaw[79] S. Rescia[21] F. Resnati[25] A. Reynolds[151] M. Ribas[187]
S. Riboldi[90] C. Riccio[182] G. Riccobene[94] L. C. J. Rice[162] J. Ricol[74]
A. Rigamonti[25] Y. Rigaut[57] D. Rivera[158] A. Robert[74]
L. Rochester[172] M. Roda[125] P. Rodrigues[151] M. J. Rodriguez
Alonso[25] E. Rodriguez Bonilla[6] J. Rodriguez Rondon[178]
S. Rosauro-Alcaraz[129] M. Rosenberg[162] P. Rosier[155] B. Roskovec[30]
M. Rossella[93,157] M. Rossi[25] C. Rott *[183,197] J. Rout[112] P. Roy[204]
S. Roy[76] A. Rubbia[57] C. Rubbia[71] F. C. Rubio[82] B. Russell[124]
D. Ruterbories[168] A. Rybnikov[110] A. Saa-Hernandez[83] R. Saakyan[196]
S. Sacerdoti[156] T. Safford[135] N. Sahu[103] P. Sala[90,25] N. Samios[21]
O. Samoylov[110] M. C. Sanchez[108] V. Sandberg[126] D. A. Sanders[140]
D. Sankey[171] S. Santana[164] M. Santos-Maldonado[164]
N. Saoulidou[10] P. Sapienza[94] C. Sarasty[41] I. Sarcevic[8] G. Savage[65]
V. Savinov[162] A. Scaramelli[93] A. Scarff[177] A. Scarpelli[21]
T. Schaffer[138] H. Schellman[150,65] S. Schifano[86,66] P. Schlabach[65]
D. Schmitz[39] K. Scholberg[54] A. Schukraft[65] E. Segreto[36]
A. Selyunin[110] C. R. Senise[195] J. Sensenig[158] M. Seoane[83]
I. Seong[30] A. Sergi[17] D. Sgalaberna[57] M. H. Shaevitz[46] S. Shafaq[112]
M. Shamma[32] R. Sharankova[193] H. R. Sharma[111] R. Sharma[21]
R. Kumar[165] T. Shaw[65] C. Shepherd-Themistocleous[171]

---

*Visitor to the collaboration

A. Sheshukov[110] S. Shin[113] I. Shoemaker[200] D. Shooltz[135]
R. Shrock[182] H. Siegel[46] L. Simard[155] F. Simon[65,132] J. Sinclair[15]
G. Sinev[178] J. Singh[128] J. Singh[128] L. Singh[27] V. Singh[27,13]
R. Sipos[25] F. W. Sippach[46] G. Sirri[84] A. Sitraka[178] K. Siyeon[40]
K. Skarpaas[172] A. Smith[35] E. Smith[104] P. Smith[104] J. Smolik[48]
M. Smy[30] E.L. Snider[65] P. Snopok[100] D. Snowden-Ifft[148] M. Soares
Nunes[186] H. Sobel[30] M. Soderberg[186] S. Sokolov[110] C. J. Solano
Salinas[105] S. Söldner-Rembold[130] S.R. Soleti[124] N. Solomey[204]
V. Solovov[122] W. E. Sondheim[126] M. Sorel[82] A. Sotnikov[110]
J. Soto-Oton[26] A. Sousa[41] K. Soustruznik[38] F. Spagliardi[151]
M. Spanu[89,136] J. Spitz[134] N. J. C. Spooner[177] K. Spurgeon[186]
R. Staley[17] M. Stancari[65] L. Stanco[92,153] R. Stanley[20] R. Stein[20]
H. M. Steiner[124] A. F. Steklain Lisbôa[187] J. Stewart[21] B. Stillwell[39]
J. Stock[178] F. Stocker[25] T. Stokes[127] M. Strait[139] T. Strauss[65]
S. Striganov[65] A. Stuart[43] J. G. Suarez[56] H. Sullivan[190]
D. Summers[140] A. Surdo[88] V. Susic[14] L. Suter[65] C. M. Sutera[85,37]
R. Svoboda[29] B. Szczerbinska[189] A. M. Szelc[58] H. A. Tanaka[172]
B. Tapia Oregui[191] A. Tapper[101] S. Tariq[65] E. Tatar[99] R. Tayloe[104]
A. M. Teklu[182] M. Tenti[84] K. Terao[172] C. A. Ternes[82]
F. Terranova[89,136] G. Testera[87] T. Thakore[41] A. Thea[171]
J. L. Thompson[177] C. Thorn[21] S. C. Timm[65] V. Tishchenko[21]
J. Todd[41] L. Tomassetti[86,66] A. Tonazzo[156] D. Torbunov[139]
M. Torti[89,136] M. Tortola[82] F. Tortorici[85,37] N. Tosi[84] D. Totani[33]
M. Toups[65] C. Touramanis[125] R. Travaglini[84] J. Trevor[34] S. Trilov[20]
A. Tripathi[190] W. H. Trzaska[114] Y. Tsai[65] Y.-T. Tsai[172]
Z. Tsamalaidze[70] K. V. Tsang[172] N. Tsverava[70] S. Tufanli[25]
C. Tull[124] E. Tyley[177] M. Tzanov[127] L. Uboldi[25] M. A. Uchida[35]
J. Urheim[104] T. Usher[172] S. Uzunyan[145] M. R. Vagins[119] P. Vahle[205]
G. A. Valdiviesso[60] E. Valencia[205] P. Valerio[84,18] Z. Vallari[34]
E. Vallazza[89] J. W. F. Valle[82] S. Vallecorsa[25] R. Van Berg[158]
R. G. Van de Water[126] F. Varanini[92] D. Vargas[81] G. Varner[78]
J. Vasel[104] S. Vasina[110] G. Vasseur[24] N. Vaughan[150] K. Vaziri[65]
S. Ventura[92] A. Verdugo[26] S. Vergani[35] M. A. Vermeulen[143]
M. Verzocchi[65] M. Vicenzi[87,69] H. Vieira de Souza[36,89] C. Vignoli[72]
C. Vilela[25] B. Viren[21] T. Vrba[48] T. Wachala[142] A. V. Waldron[101]
M. Wallbank[41] C. Wallis[45] H. Wang[31] J. Wang[178] L. Wang[124]
M.H.L.S. Wang[65] Y. Wang[31] Y. Wang[182] K. Warburton[108]
D. Warner[45] M.O. Wascko[101] D. Waters[196] A. Watson[17]
P. Weatherly[53] A. Weber[171,151] M. Weber[15] H. Wei[21]

A. Weinstein[108] **D. Wenman**[206] **M. Wetstein**[108] **A. White**[190]
L. H. Whitehead[35] **D. Whittington**[186] **M. J. Wilking**[182]
C. Wilkinson[124] **Z. Williams**[190] **F. Wilson**[171] **R. J. Wilson**[45]
W. Wisniewski[172] **J. Wolcott**[193] **T. Wongjirad**[193] **A. Wood**[79]
K. Wood[182] **E. Worcester**[21] **M. Worcester**[21] **C. Wret**[168] **W. Wu**[65]
W. Wu[30] **Y. Xiao**[30] **F. Xie**[185] **E. Yandel**[33] **G. Yang**[182] **K. Yang**[151]
S. Yang[41] **T. Yang**[65] **A. Yankelevich**[30] **N. Yershov**[95] **K. Yonehara**[65]
T. Young[144] **B. Yu**[21] **H. Yu**[21] **H. Yu**[184] **J. Yu**[190] **W. Yuan**[58] **R. Zaki**[209]
J. Zalesak[47] **L. Zambelli**[51] **B. Zamorano**[73] **A. Zani**[90] **L. Zazueta**[205]
G. P. Zeller[65] **J. Zennamo**[65] **K. Zeug**[206] **C. Zhang**[21] **M. Zhao**[21]
E. Zhivun[21] **G. Zhu**[149] **P. Zilberman**[182] **E. D. Zimmerman**[44]
M. Zito[24] **S. Zucchelli**[84,18] **J. Zuklin**[47] **V. Zutshi**[145] **and R. Zwaska**[65]

[1]Abilene Christian University, Abilene, TX 79601, USA

[2]University of Albany, SUNY, Albany, NY 12222, USA

[3]University of Amsterdam, NL-1098 XG Amsterdam, The Netherlands

[4]Antalya Bilim University, 07190 Döşemealtı/Antalya, Turkey

[5]University of Antananarivo, Antananarivo 101, Madagascar

[6]Universidad Antonio Nariño, Bogotá, Colombia

[7]Argonne National Laboratory, Argonne, IL 60439, USA

[8]University of Arizona, Tucson, AZ 85721, USA

[9]Universidad Nacional de Asunción, San Lorenzo, Paraguay

[10]University of Athens, Zografou GR 157 84, Greece

[11]Universidad del Atlántico, Barranquilla, Atlántico, Colombia

[12]Augustana University, Sioux Falls, SD 57197, USA

[13]Banaras Hindu University, Varanasi - 221 005, India

[14]University of Basel, CH-4056 Basel, Switzerland

[15]University of Bern, CH-3012 Bern, Switzerland

[16]Beykent University, Istanbul, Turkey

[17]University of Birmingham, Birmingham B15 2TT, United Kingdom

[18]Università del Bologna, 40127 Bologna, Italy

[19]Boston University, Boston, MA 02215, USA

[20]University of Bristol, Bristol BS8 1TL, United Kingdom

[21]Brookhaven National Laboratory, Upton, NY 11973, USA

[22]University of Bucharest, Bucharest, Romania

[23]Centro Brasileiro de Pesquisas Físicas, Rio de Janeiro, RJ 22290-180, Brazil

[24]IRFU, CEA, Université Paris-Saclay, F-91191 Gif-sur-Yvette, France

[25]CERN, The European Organization for Nuclear Research, 1211 Meyrin, Switzerland

[26]CIEMAT, Centro de Investigaciones Energéticas, Medioambientales y Tecnológicas, E-28040 Madrid, Spain

[27]Central University of South Bihar, Gaya, 824236, India

[28]University of California Berkeley, Berkeley, CA 94720, USA

[29] University of California Davis, Davis, CA 95616, USA

[30] University of California Irvine, Irvine, CA 92697, USA

[31] University of California Los Angeles, Los Angeles, CA 90095, USA

[32] University of California Riverside, Riverside CA 92521, USA

[33] University of California Santa Barbara, Santa Barbara, California 93106 USA

[34] California Institute of Technology, Pasadena, CA 91125, USA

[35] University of Cambridge, Cambridge CB3 0HE, United Kingdom

[36] Universidade Estadual de Campinas, Campinas - SP, 13083-970, Brazil

[37] Università di Catania, 2 - 95131 Catania, Italy

[38] Institute of Particle and Nuclear Physics of the Faculty of Mathematics and Physics of the Charles University, 180 00 Prague 8, Czech Republic

[39] University of Chicago, Chicago, IL 60637, USA

[40] Chung-Ang University, Seoul 06974, South Korea

[41] University of Cincinnati, Cincinnati, OH 45221, USA

[42] Centro de Investigación y de Estudios Avanzados del Instituto Politécnico Nacional (Cinvestav), Mexico City, Mexico

[43] Universidad de Colima, Colima, Mexico

[44] University of Colorado Boulder, Boulder, CO 80309, USA

[45] Colorado State University, Fort Collins, CO 80523, USA

[46] Columbia University, New York, NY 10027, USA

[47] Institute of Physics, Czech Academy of Sciences, 182 00 Prague 8, Czech Republic

[48] Czech Technical University, 115 19 Prague 1, Czech Republic

[49] Dakota State University, Madison, SD 57042, USA

[50] University of Dallas, Irving, TX 75062-4736, USA

[51] Laboratoire d'Annecy de Physique des Particules, Univ. Grenoble Alpes, Univ. Savoie Mont Blanc, CNRS, LAPP-IN2P3, 74000 Annecy, France

[52] Daresbury Laboratory, Cheshire WA4 4AD, United Kingdom

[53] Drexel University, Philadelphia, PA 19104, USA

[54] Duke University, Durham, NC 27708, USA

[55] Durham University, Durham DH1 3LE, United Kingdom

[56] Universidad EIA, Envigado, Antioquia, Colombia

[57] ETH Zurich, Zurich, Switzerland

[58] University of Edinburgh, Edinburgh EH8 9YL, United Kingdom

[59] Faculdade de Ciências da Universidade de Lisboa - FCUL, 1749-016 Lisboa, Portugal

[60] Universidade Federal de Alfenas, Poços de Caldas - MG, 37715-400, Brazil

[61] Universidade Federal de Goias, Goiania, GO 74690-900, Brazil

[62] Universidade Federal de São Carlos, Araras - SP, 13604-900, Brazil

[63] Universidade Federal do ABC, Santo André - SP, 09210-580, Brazil

[64] Universidade Federal do Rio de Janeiro, Rio de Janeiro - RJ, 21941-901, Brazil

[65] Fermi National Accelerator Laboratory, Batavia, IL 60510, USA

[66] University of Ferrara, Ferrara, Italy

[67] University of Florida, Gainesville, FL 32611-8440, USA

[68] Fluminense Federal University, 9 Icaraí Niterói - RJ, 24220-900, Brazil

[69]Università degli Studi di Genova, Genova, Italy

[70]Georgian Technical University, Tbilisi, Georgia

[71]Gran Sasso Science Institute, L'Aquila, Italy

[72]Laboratori Nazionali del Gran Sasso, L'Aquila AQ, Italy

[73]University of Granada & CAFPE, 18002 Granada, Spain

[74]University Grenoble Alpes, CNRS, Grenoble INP, LPSC-IN2P3, 38000 Grenoble, France

[75]Universidad de Guanajuato, Guanajuato, C.P. 37000, Mexico

[76]Harish-Chandra Research Institute, Jhunsi, Allahabad 211 019, India

[77]Harvard University, Cambridge, MA 02138, USA

[78]University of Hawaii, Honolulu, HI 96822, USA

[79]University of Houston, Houston, TX 77204, USA

[80]University of Hyderabad, Gachibowli, Hyderabad - 500 046, India

[81]Institut de Física d'Altes Energies (IFAE)—Barcelona Institute of Science and Technology (BIST), Barcelona, Spain

[82]Instituto de Física Corpuscular, CSIC and Universitat de València, 46980 Paterna, Valencia, Spain

[83]Instituto Galego de Fisica de Altas Enerxias, A Coruña, Spain

[84]Istituto Nazionale di Fisica Nucleare Sezione di Bologna, 40127 Bologna BO, Italy

[85]Istituto Nazionale di Fisica Nucleare Sezione di Catania, I-95123 Catania, Italy

[86]Istituto Nazionale di Fisica Nucleare Sezione di Ferrara, I-44122 Ferrara, Italy

[87]Istituto Nazionale di Fisica Nucleare Sezione di Genova, 16146 Genova GE, Italy

[88]Istituto Nazionale di Fisica Nucleare Sezione di Lecce, 73100 - Lecce, Italy

[89]Istituto Nazionale di Fisica Nucleare Sezione di Milano Bicocca, 3 - I-20126 Milano, Italy

[90]Istituto Nazionale di Fisica Nucleare Sezione di Milano, 20133 Milano, Italy

[91]Istituto Nazionale di Fisica Nucleare Sezione di Napoli, I-80126 Napoli, Italy

[92]Istituto Nazionale di Fisica Nucleare Sezione di Padova, 35131 Padova, Italy

[93]Istituto Nazionale di Fisica Nucleare Sezione di Pavia, I-27100 Pavia, Italy

[94]Istituto Nazionale di Fisica Nucleare Laboratori Nazionali del Sud, 95123 Catania, Italy

[95]Institute for Nuclear Research of the Russian Academy of Sciences, Moscow 117312, Russia

[96]Institut de Physique des 2 Infinis de Lyon, 69622 Villeurbanne, France

[97]Institute for Research in Fundamental Sciences, Tehran, Iran

[98]Instituto Superior Técnico - IST, Universidade de Lisboa, Portugal

[99]Idaho State University, Pocatello, ID 83209, USA

[100]Illinois Institute of Technology, Chicago, IL 60616, USA

[101]Imperial College of Science Technology and Medicine, London SW7 2BZ, United Kingdom

[102]Indian Institute of Technology Guwahati, Guwahati, 781 039, India

[103]Indian Institute of Technology Hyderabad, Hyderabad, 502285, India

[104]Indiana University, Bloomington, IN 47405, USA

[105]Universidad Nacional de Ingeniería, Lima 25, Perú

[106]University of Insubria, Via Ravasi, 2, 21100 Varese VA, Italy

[107]University of Iowa, Iowa City, IA 52242, USA

[108]Iowa State University, Ames, Iowa 50011, USA

[109]Iwate University, Morioka, Iwate 020-8551, Japan

[110]Joint Institute for Nuclear Research, Dzhelepov Laboratory of Nuclear Problems 6 Joliot-Curie, Dubna, Moscow Region, 141980 RU

[111]University of Jammu, Jammu-180006, India

[112]Jawaharlal Nehru University, New Delhi 110067, India

[113]Jeonbuk National University, Jeonrabuk-do 54896, South Korea

[114]University of Jyvaskyla, FI-40014, Finland

[115]High Energy Accelerator Research Organization (KEK), Ibaraki, 305-0801, Japan

[116]Korea Institute of Science and Technology Information, Daejeon, 34141, South Korea

[117]K L University, Vaddeswaram, Andhra Pradesh 522502, India

[118]Kansas State University, Manhattan, KS 66506, USA

[119]Kavli Institute for the Physics and Mathematics of the Universe, Kashiwa, Chiba 277-8583, Japan

[120]National Institute of Technology, Kure College, Hiroshima, 737-8506, Japan

[121]Taras Shevchenko National University of Kyiv, 01601 Kyiv, Ukraine

[122]Laboratório de Instrumentação e Física Experimental de Partículas, 1649-003 Lisboa and 3004-516 Coimbra, Portugal

[123]Lancaster University, Lancaster LA1 4YB, United Kingdom

[124]Lawrence Berkeley National Laboratory, Berkeley, CA 94720, USA

[125]University of Liverpool, L69 7ZE, Liverpool, United Kingdom

[126]Los Alamos National Laboratory, Los Alamos, NM 87545, USA

[127]Louisiana State University, Baton Rouge, LA 70803, USA

[128]University of Lucknow, Uttar Pradesh 226007, India

[129]Madrid Autonoma University and IFT UAM/CSIC, 28049 Madrid, Spain

[130]University of Manchester, Manchester M13 9PL, United Kingdom

[131]Massachusetts Institute of Technology, Cambridge, MA 02139, USA

[132]Max-Planck-Institut, Munich, 80805, Germany

[133]University of Medellín, Medellín, 050026 Colombia

[134]University of Michigan, Ann Arbor, MI 48109, USA

[135]Michigan State University, East Lansing, MI 48824, USA

[136]Università del Milano-Bicocca, 20126 Milano, Italy

[137]Università degli Studi di Milano, I-20133 Milano, Italy

[138]University of Minnesota Duluth, Duluth, MN 55812, USA

[139]University of Minnesota Twin Cities, Minneapolis, MN 55455, USA

[140]University of Mississippi, University, MS 38677 USA

[141]University of New Mexico, Albuquerque, NM 87131, USA

[142]H. Niewodniczański Institute of Nuclear Physics, Polish Academy of Sciences, Cracow, Poland

[143]Nikhef National Institute of Subatomic Physics, 1098 XG Amsterdam, Netherlands

[144]University of North Dakota, Grand Forks, ND 58202-8357, USA

[145]Northern Illinois University, DeKalb, IL 60115, USA

[146]Northwestern University, Evanston, Il 60208, USA

[147]University of Notre Dame, Notre Dame, IN 46556, USA

[148]Occidental College, Los Angeles, CA 90041

[149]Ohio State University, Columbus, OH 43210, USA

[150]Oregon State University, Corvallis, OR 97331, USA

[151]University of Oxford, Oxford, OX1 3RH, United Kingdom

[152]Pacific Northwest National Laboratory, Richland, WA 99352, USA

[153]Universtà degli Studi di Padova, I-35131 Padova, Italy

[154]Panjab University, Chandigarh, 160014 U.T., India

[155]Université Paris-Saclay, CNRS/IN2P3, IJCLab, 91405 Orsay, France

[156]Université de Paris, CNRS, Astroparticule et Cosmologie, F-75006, Paris, France

[157]Università degli Studi di Pavia, 27100 Pavia PV, Italy

[158]University of Pennsylvania, Philadelphia, PA 19104, USA

[159]Pennsylvania State University, University Park, PA 16802, USA

[160]Physical Research Laboratory, Ahmedabad 380 009, India

[161]Università di Pisa, I-56127 Pisa, Italy

[162]University of Pittsburgh, Pittsburgh, PA 15260, USA

[163]Pontificia Universidad Católica del Perú, Lima, Perú

[164]University of Puerto Rico, Mayaguez 00681, Puerto Rico, USA

[165]Punjab Agricultural University, Ludhiana 141004, India

[166]Queen Mary University of London, London E1 4NS, United Kingdom

[167]Radboud University, NL-6525 AJ Nijmegen, Netherlands

[168]University of Rochester, Rochester, NY 14627, USA

[169]Royal Holloway College London, TW20 0EX, United Kingdom

[170]Rutgers University, Piscataway, NJ, 08854, USA

[171]STFC Rutherford Appleton Laboratory, Didcot OX11 0QX, United Kingdom

[172]SLAC National Accelerator Laboratory, Menlo Park, CA 94025, USA

[173]Sanford Underground Research Facility, Lead, SD, 57754, USA

[174]Università del Salento, 73100 Lecce, Italy

[175]San Jose State University, San José, CA 95192-0106, USA

[176]Universidad Sergio Arboleda, 11022 Bogotá, Colombia

[177]University of Sheffield, Sheffield S3 7RH, United Kingdom

[178]South Dakota School of Mines and Technology, Rapid City, SD 57701, USA

[179]South Dakota State University, Brookings, SD 57007, USA

[180]University of South Carolina, Columbia, SC 29208, USA

[181]Southern Methodist University, Dallas, TX 75275, USA

[182]Stony Brook University, SUNY, Stony Brook, NY 11794, USA

[183]Sungkyunkwan University, Suwon, 16419, Korea, visitor to the collaboration

[184]Sun Yat-Sen University, Guangzhou, 510275

[185]University of Sussex, Brighton, BN1 9RH, United Kingdom

[186]Syracuse University, Syracuse, NY 13244, USA

[187]Universidade Tecnológica Federal do Paraná, Curitiba, Brazil

[188]Texas A&M University, College Station, Texas 77840

[189]Texas A&M University - Corpus Christi, Corpus Christi, TX 78412, USA

[190]University of Texas at Arlington, Arlington, TX 76019, USA

[191]University of Texas at Austin, Austin, TX 78712, USA

[192]University of Toronto, Toronto, Ontario M5S 1A1, Canada

[193]Tufts University, Medford, MA 02155, USA

[194]Ulsan National Institute of Science and Technology, Ulsan 689-798, South Korea

[195]Universidade Federal de São Paulo, 09913-030, São Paulo, Brazil

[196]University College London, London, WC1E 6BT, United Kingdom

[197]University of Utah, Salt Lake City, UT 84112, USA, visitor to the collaboration

[198]Valley City State University, Valley City, ND 58072, USA

[199]Variable Energy Cyclotron Centre, 700 064 West Bengal, India

[200]Virginia Tech, Blacksburg, VA 24060, USA

[201]University of Warsaw, 02-093 Warsaw, Poland

[202]University of Warwick, Coventry CV4 7AL, United Kingdom

[203]Wellesley College, Wellesley, MA 02481, USA

[204]Wichita State University, Wichita, KS 67260, USA

[205]William and Mary, Williamsburg, VA 23187, USA

[206]University of Wisconsin Madison, Madison, WI 53706, USA

[207]Yale University, New Haven, CT 06520, USA

[208]Yerevan Institute for Theoretical Physics and Modeling, Yerevan 0036, Armenia

[209]York University, Toronto M3J 1P3, Canada

E-mail: dune-www-pubs@fnal.gov

Abstract. The observation of 236 MeV muon neutrinos from kaon-decay-at-rest (KDAR) originating in the core of the Sun would provide a unique signature of dark matter annihilation. Since excellent angle and energy reconstruction are necessary to detect this monoenergetic, directional neutrino flux, DUNE with its vast volume and reconstruction capabilities, is a promising candidate for a KDAR neutrino search. In this work, we evaluate the proposed KDAR neutrino search strategies by realistically modeling both neutrino-nucleus interactions and the response of DUNE. We find that, although reconstruction of the neutrino energy and direction is difficult with current techniques in the relevant energy range, the superb energy resolution, angular resolution, and particle identification offered by DUNE can still permit great signal/background discrimination. Moreover, there are non-standard scenarios in which searches at DUNE for KDAR in the Sun can probe dark matter interactions.

Keywords: Dark matter, Solar WIMPs, indirect WIMP search

Contents

1 Introduction

There has been recent interest from the experimental community in detecting the neutrinos produced by kaon decay at rest (KDAR) [1, 2]. One application for these techniques is the search for neutrinos produced when gravitationally-captured dark matter annihilates in the core of the Sun [3–5]. If dark matter annihilation produces u, d, and s quarks, then the result of subsequent hadronization and fragmentation would be a large number of K^+ which come to rest in the dense solar medium before decaying. 64% of these decays ($K^+ \to \mu^+\nu_\mu$) produce monoenergetic ν_μ with an energy of $\sim$ 236 MeV [6–8]. The oscillations of these neutrinos while passing through the dense solar medium and vacuum results in approximately comparable fluxes of active neutrinos in all three flavors at Earth [9]. Recent work has focused on developing new techniques for utilizing the excellent particle identification and energy and angular resolution of DUNE to identify the energy and direction of the incoming 236 MeV neutrino [10]. The identification of a flux of 236 MeV neutrinos arriving from the Sun would be an extraordinary signal of new physics, providing a new handle on dark matter interactions which could be a unique probe of non-standard dark matter models [11]. This work further develops techniques for measuring the monoenergetic neutrinos arising from KDAR in the Sun, with a focus on increasing the signal-to-background ratio.

At water Cherenkov (WC) neutrino detectors, it is very difficult to determine the direction of an $\mathcal{O}(100)$ MeV neutrino because the charged lepton produced by a charged-current interaction is largely isotropic at these energies. But in a large fraction of neutrino-argon CC-interactions, a proton is ejected preferentially in the forward direction. Though this proton cannot be seen in a WC detector, its energy and direction can be well-measured in a liquid argon time projection chamber (LArTPC) detector, such as DUNE. Thus, although WC detectors will generally have a statistical advantage due to their size, LArTPC detectors can have an advantage in reducing some systematic uncertainties, due to a greater ability to reject background.

In [10], it was proposed that one search for DUNE events with exactly one proton and one charged lepton with a total energy of 236 MeV, and with the proton directed away from the Sun. It was found that this directionality strategy should improve DUNE sensitivity to dark

matter annihilation in the Sun, while yielding a signal-to-background ratio as high as $\sim 40\%$. In this paper, we use the LArSoft package [14] to realistically model the detector response, including the asymmetric response due to the orientation of the detector with respect to the incoming neutrino, and we use the Pandora package [16] to perform track reconstruction. We also find that, although the charged lepton is produced roughly isotropically, its direction is correlated with that of the proton, providing a new method for rejecting background that can significantly improve the signal-to-background ratio.

At DUNE, the charged current interaction $\nu_\ell + {}^{40}\text{Ar} \to \ell^- + p^+ + {}^{39}\text{Ar}$ produces an ejected proton and charged lepton which can be well-measured [12]. But the recoil of the remnant ${}^{39}\text{Ar}$ will not be well-measured, and although the kinetic energy of the remnant nucleus will be small, its momentum may be substantial. But given a hypothesis for the energy and momentum of the neutrino (i. e., a 236 MeV neutrino arriving from the Sun), the momentum of the remnant nucleus can be reconstructed using momentum conservation. We find that when the struck proton is very forward-directed, the remnant nucleus is typically backscattered (more on this in Section 2 and Fig. 10). Utilizing this correlation, we find that for models where evidence can be found at 90% C.L. with a 400 kT yr exposure of DUNE, the signal-to-background ratio can be as high as 2.2.

We find that, with a 400 kT yr exposure, DUNE can probe $\mathcal{O}(10^3)\ \text{m}^{-2}\ \text{s}^{-1}$ fluxes of 236 MeV ν_μ emanating from the Sun. As a specific example, we consider the case of low-mass dark matter ($m \lesssim 10\ \text{GeV}$) which scatters inelastically with nuclei. We estimate the sensitivity of DUNE to models which cannot be probed by direct detection experiments.

The plan of this paper is as follows. In Section 2, we describe our simulation framework and analysis cuts. In Section 3, we describe the resulting sensitivity to a flux of KDAR neutrinos, and as an example, interpret this as a sensitivity to a particular class of dark matter models which cannot be probed by direct detection experiments. We conclude with a discussion of our results in Section 4.

2   Event Simulation and Analysis Cuts

Dark matter annihilation at the core of the Sun can produce light mesons, whose decays-at-rest can produce monoenergetic neutrinos. KDAR ($K^+ \to \mu^+ \nu_\mu$) will produce a $E_\nu = 236$ MeV monoenergetic ν_μ at the core of the Sun. On the other hand, K^- and π^- will tend to be Coulomb-captured by nuclei. Hence the flux of neutrinos from K^- and π^- is small [17]. π^+ decay-at-rest in the Sun will produce a monoenergetic 30 MeV neutrino. But this signal is less promising [8], because the background from atmospheric neutrinos is larger at these energies, while the $\nu - {}^{40}\text{Ar}$ cross section is smaller. Moreover, the scattering of a 30 MeV neutrino is less likely to eject a proton, which is needed for directionality. Dark matter annihilation can also produce muons which decay at rest, but this signal is less promising because it does not yield a monoenergetic neutrino. As a result, we focus on the 236 MeV ν_μ produced by KDAR in the Sun.

By the time this neutrino reaches Earth, it will have oscillated into all three flavors. But only ν_μ and ν_e can produce a charged-current interaction at this energy. In this analysis, we only consider ν_μ. We are interested in charge-current events in which a muon is produced and a proton is ejected from the nucleus, since these particles can leave crisp tracks in DUNE, as shown in Fig. 1.
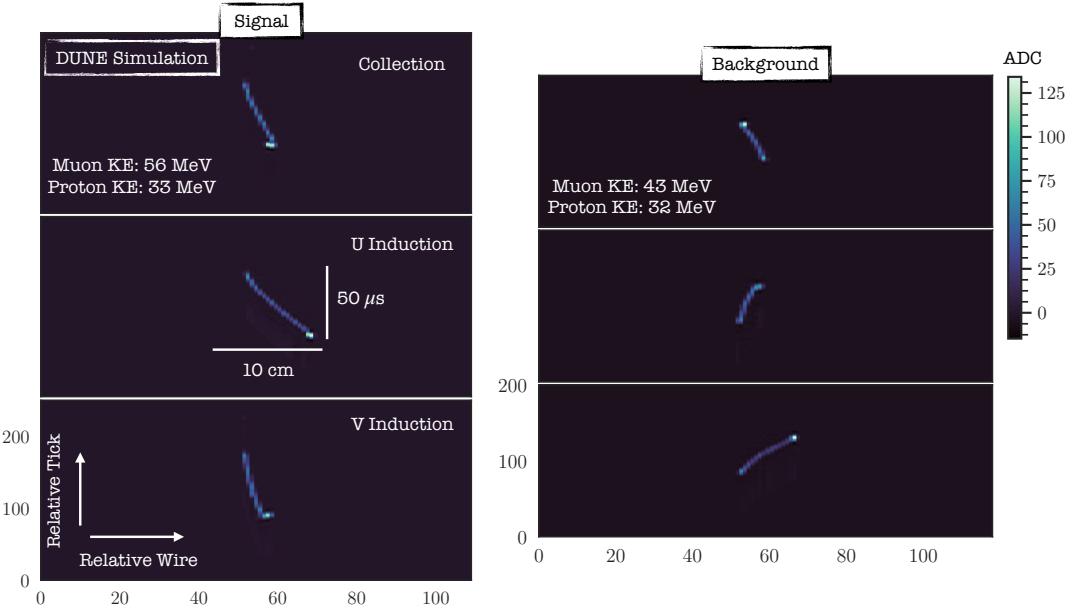
Figure 1. Time (ticks) vs. wire (number) view of a 236 MeV ν_μ event simulated at DUNE. The color corresponds to the voltage read out on the wires (in ADCs). Each tick is 500 ns. Each panel corresponds to an individual wire plane. The wire spacing for the top (collection) plane is 4.79 mm. The wire spacing for the middle and bottom (induction) planes is 4.67 mm. The collection plane is aligned with the vertical of the detector frame and the induction planes are angled 35.7° with respect to vertical. A muon and a proton are ejected. The muon is the longest track. Fig. 2 shows the distributions of the kinetic energies of the ejected protons and muons. The right panel shows a background event stemming from a neutrino of 190 MeV.
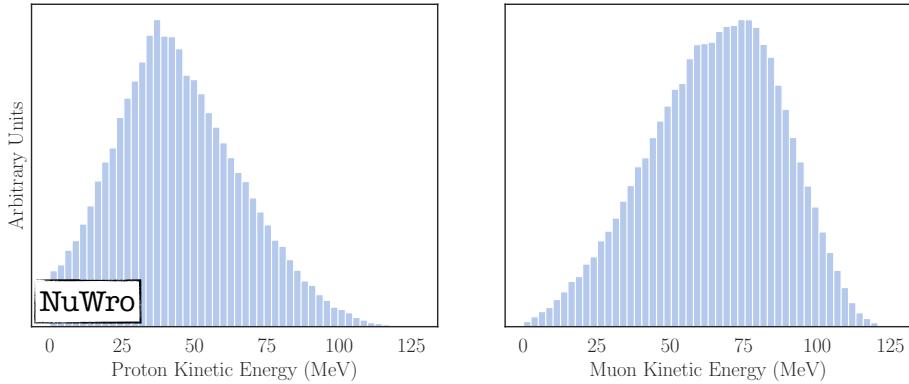
Figure 2. NuWro [18] generated proton and muon kinetic energies for the 1 proton + 1 muon = 2 total particles case. Generally, if we do not enforce a 2 particle cap, 13% of the CC events are multi-proton at generator level. 76% are single proton. 10% are without protons.

2.1 Event Generation

We use NuWro [18] to simulate neutrino-nucleus scattering events because it allows us to model the nuclear response using a spectral function to simulate the nucleus [20], rather than the Fermi Gas model . Final state interactions are modeled using an intra-nuclear

cascade (INC) [21]. At 236 MeV, the NuWro neutrino event generator predicts a 4% MEC (meson exchange current) contribution, a 32% NCQE (neutral current quasi-elastic) contribution, and a 64% CCQE (charged current quasi-elastic) contribution to the neutrino-argon scattering cross section, with a negligible contribution for all other processes (pions are produced 0.04% of the time). However, neutral current interactions do not eject muons. We do not include NC in our analysis because we expect excellent muon identification in DUNE and hence very few NC events in which a muon is identified. This expectation is motivated by the success of the dE/dx vs. residual range method at ProtoDUNE-SP (as shown in [13]). At 236 MeV, neutrino charged-current interactions with nucleons are mostly quasi-elastic (CCQE), $\nu_\ell + n \to \ell^- + p^+$. Fig. 2 shows the expected distribution, generated by NuWro, of the kinetic energies of the muons and protons produced by charged current interactions of a 236 MeV ν_μ.

Thus, we are interested in charged-current quasi-elastic (CCQE) $\nu_\mu + {}^{40}Ar$ interactions. We simulate CCQE signal events - 236 MeV neutrinos arriving from the direction of the Sun - and background events (atmospheric neutrino events, assumed to be isotropic) in NuWro. We do not consider non-DM KDAR in the Sun as a background. True, cosmic rays impinge on the Sun and produce KDAR but this contribution is negligible [8].

For signal events, the neutrino is assumed to arrive from the direction of the Sun, but at a randomized time (which determines the orientation of the Sun with respect to the detector). For an atmospheric neutrino background event, the orientation of the neutrino with respect to the detector is randomized. The distribution of signal event directions relative to the detector are show in Fig. 3. In particular, and unlike atmospheric neutrinos, neutrinos arriving from the Sun cannot have an arbitrary orientation with respect to the detector wires, but must instead arrive from directions within the yellow band of Fig. 3.
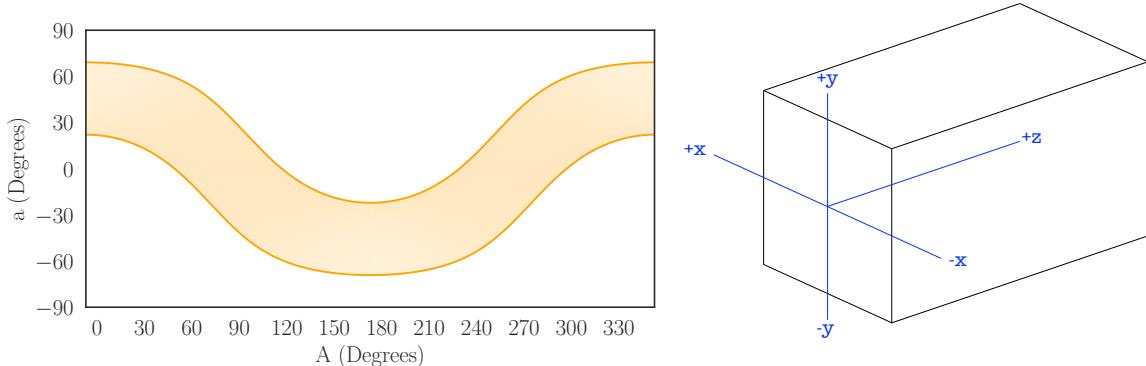

Figure 3. Solar directions (a = altitude, A = azimuth) seen at DUNE. The band is the finite angular coverage of the Sun. Azimuth winds clockwise from $\hat{x}$ to $\hat{z}$ in the detector frame and altitude goes up from the xz plane to $\hat{y}$. Note, these angles are often defined respect to the cardinal directions rather than the detector.

2.2 Event Simulation and Reconstruction

In each event, the particles generated with NuWro serve as input for LArSoft [14], which propagates the particles through argon (using GEANT4 [15]) and simulates the detector response to the drifted ionization electrons. LArSoft also searches the simulated TPC wire waveforms for regions of interest and deconvolves and fits them to a Gaussian. These cleaned

up "hits" are 2D (each plane of wires is an image of ticks vs. wire) and are shown in Fig 1. Finally, Pandora [16], a pattern recognition software kit, maps the 2D hits from the 3 wire plane projections to 3D and then clusters the 3D positions into tracks and showers.

2.3 Energy and Angular Resolution

We can estimate the angular resolution with which proton and muon tracks can be reconstructed by comparing the direction of the outgoing particle at the event generator level to the direction of the fully reconstructed tracks. We find that roughly 50% of tracks are reconstructed to within 5° of the true particle direction (Fig. 4). Furthermore, we infer the particle momenta via "range" (track length). Fig. 5 compares the true (GEANT4) and the reconstructed track lengths and gives us faith in this method. The true track length is the distance over which GEANT4 propagates the particle before it stops or decays, while the reconstructed track length is based on the hits generated by the ions created by this particle.
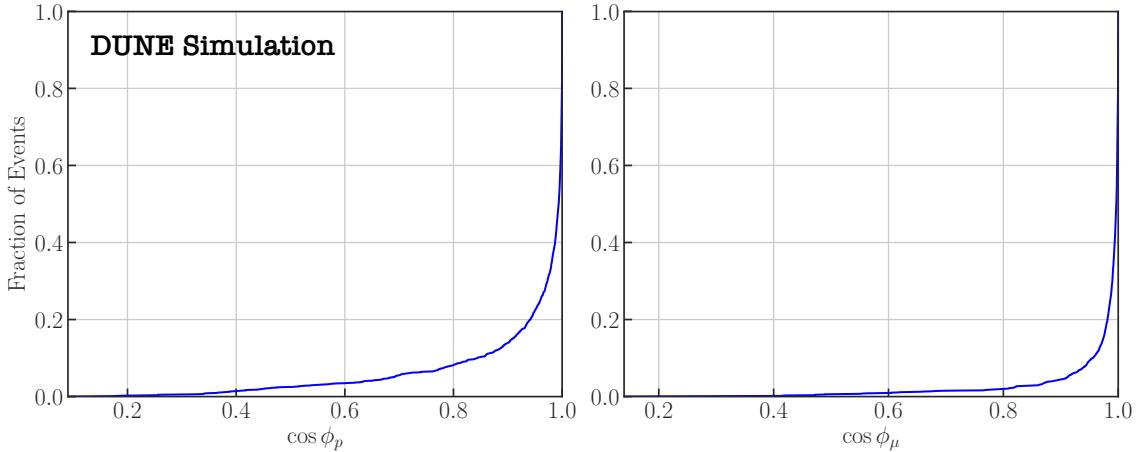
Figure 4. Cumulative distribution functions of the angular difference between the true and reconstructed track directions. ϕ_p is the proton angular difference and ϕ_μ is the muon angular difference.

The charge read out on the LArTPC wires can be mapped to the kinetic energy of the culprit particle which caused the ionization. For events in which a proton and muon track are identified, we can measure the proton and muon energies, including the particle rest mass and the kinetic energy.

We reconstruct the ν_μ energy using the expression

$$E_{\nu_\mu}^{\text{recon}} \equiv E_p + E_\mu + (m_{\text{Ar}}^{39} - m_{\text{Ar}}^{40}). \tag{2.1}$$

In Fig. 6, we plot the distribution of reconstructed neutrino energies for events in which a 236 MeV ν_μ charged-current interaction is simulated in NuWro. The reconstructed neutrino energies are well clustered around the true energy of 236 MeV, with a variance of 30 MeV. Eq. 2.1 does not include the kinetic energy of the remnant ^{39}Ar. Although the maximum momentum transfer to the nucleus is $\mathcal{O}(200)$ MeV, the maximum recoil energy is $\mathcal{O}(1)$ MeV, which is negligible compared to the 30 MeV energy resolution.
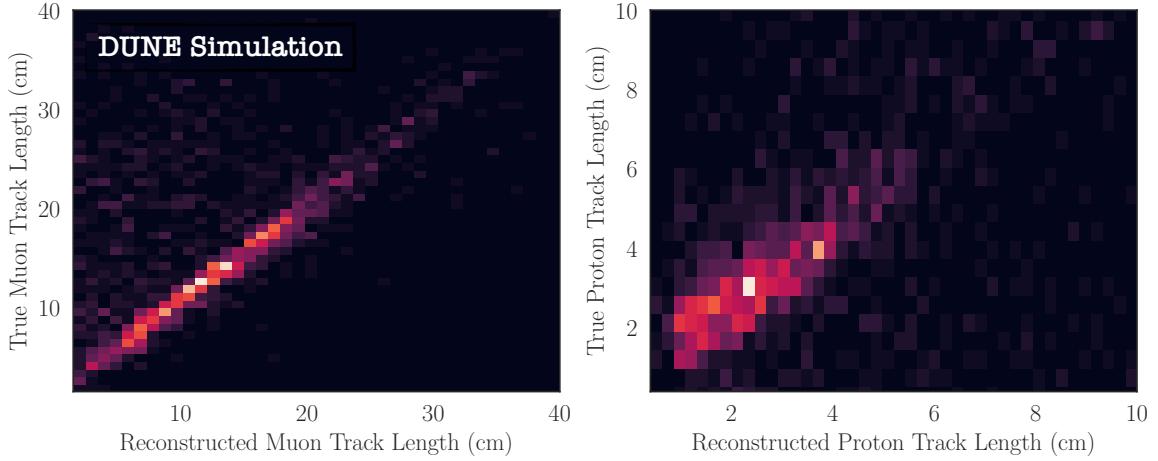
Figure 5. Comparison of the true (GEANT4) and the reconstructed track lengths for the muon (left) and proton (right). This analysis uses the track lengths to infer the proton and muon momenta.
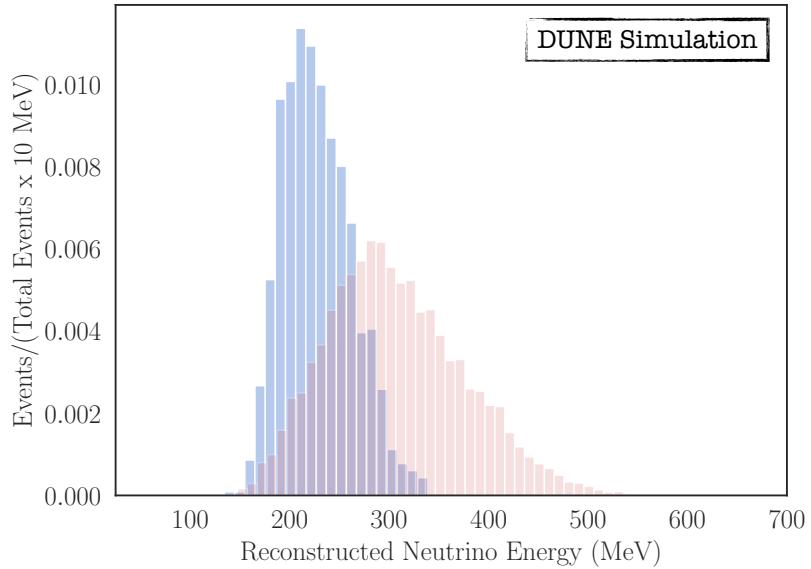

Figure 6. Distribution of the reconstructed neutrino energies. The blue histogram shows events with a true energy of 236 MeV, while the red histogram corresponds to the atmospheric background in the 150-400 MeV range. The area of both distributions is normalized to 1. The signal (blue) has a standard deviation of ±30 MeV. This informs our choice of the relevant background energy - true energies between 150 and 400 MeV - a range 3 times larger than the reconstructed signal energy resolution.

2.4 Event Selection

The atmospheric neutrinos are taken to have energies between 150 MeVand 400 MeV, with an angle-averaged energy spectrum[*] calculated for Homestake at the solar minimum [19]. We choose this background energy range in order to encompass 3 standard deviations of the reconstructed signal energy. We are justified in ignoring atmospheric neutrinos whose true energies lie outside this range, since they can be well distinguished from the signal by reconstruction of the neutrino energy.

NuWro reports the neutrino-nucleus CCQE cross section; for signal events it reports the cross section at $E_{\nu_\mu} = 236$ MeV, and for atmospheric neutrinos it reports the average cross section weighted by the neutrino energy spectrum between 150 MeVand 400 MeV.

These cross sections are

$$\sigma^{sig}_{\nu_\mu - ^{40}\mathrm{Ar}} = 2.6 \times 10^{-38} \ \ \mathrm{cm}^2,$$
$$\sigma^{bgd.}_{\nu_\mu - ^{40}\mathrm{Ar}} = 2.8 \times 10^{-38} \ \ \mathrm{cm}^2. \tag{2.2}$$

In simulating the CC cross section, we only have events with produced muons, and with neutrinos in the aforementioned energy range. The CCQE cross section is weighted and averaged only over this range. We have not simulated neutral current events, because such events do not produce a muon.

As an initial event selection cut, we consider events in which exactly two tracks are reconstructed, that of a muon and a proton. Although it is expected that DUNE will have excellent particle identification, for simplicity, we only require that Pandora identify exactly two tracks, and we assume that the longer track is a muon while the shorter track is a proton. At 236 MeV, GEANT4 predicts this to be the case 93% of the time. Out of these 93%, 97% are correctly reconstructed as the longer track. Also, a small number of events passing the cuts contain additional ejected nucleons at the event generator level, but for which only one nucleon track was reconstructed.

The requirement that we reconstruct the interaction with an interaction point within the fiducial volume justifies our assumption that the dominant background arises from atmospheric neutrinos. There are a variety of other cosmogenic backgrounds at DUNE, but these backgrounds are unlikely to produce an identified muon track which is reconstructed to begin within the detector. In other words, we have assumed that the analysis is based on a fiducial volume chosen such that the rate of such backgrounds is negligible.

2.5 Neutrino directionality

Since the momentum transfer to $^{39}\mathrm{Ar}$ is non-negligible, one cannot use $\vec{p}_\mu$ and $\vec{p}_p$ to reconstruct the direction of the incoming neutrino.[†] Instead we note that, given a hypothesis for the direction of the incoming neutrino, one can use momentum conservation to determine

---

[*]Besides an angle-averaged spectrum, [19] provides direction-dependent fluxes binned in the cosine of the zenith angle, Z, and azimuth, ϕ. The fractional variance of the direction-dependent fluxes compared to the angle-averaged flux decreases with energy for the energies relevant to this study. At 236 (600) MeV, it is 0.34 (0.19). In using the average, the maximum overestimate at 236 MeV is a factor of 3.7. This happens between (-0.8,-0.9) in $\cos(Z)$ and between (90,120) degrees in ϕ. The maximum underestimate is by a factor of 2.2. This happens between (0, 0.1) in $\cos(Z)$ and between (270, 300) degrees in ϕ.

[†]Note, for higher energy neutrinos, the momentum transfer to the remnant nucleus is negligible compared to the energy of neutrino, in which case the momentum of the charged lepton and of the hadronic ejecta is sufficient to reconstruct the neutrino direction effectively. These techniques were used in [22].

the momentum transfer to the remnant nucleus. We define the kinematic variable

$$\vec{p}_{^{39}\mathrm{Ar}} \equiv (236 \ \mathrm{MeV})\hat{p}_{\odot} - \vec{p}_{\mu} - \vec{p}_{p}, \tag{2.3}$$

where $\hat{p}_{\odot}$ is a unit vector pointing from the Sun to the detector. If the incoming 236 MeV neutrino were actually arriving from the Sun, then $\vec{p}_{^{39}\mathrm{Ar}}$ would be the reconstructed momentum of the remnant nucleus.

As noted in [10], the ejected proton tends to emerge preferentially in the forward direction. As such, the angle θ_p between the proton and the direction from the Sun, defined by $\cos\theta_p = (\hat{p}_{\odot} \cdot \vec{p}_p)/|\vec{p}_p|$, is one of the kinematic variables upon which we will impose cuts (Fig. 7).
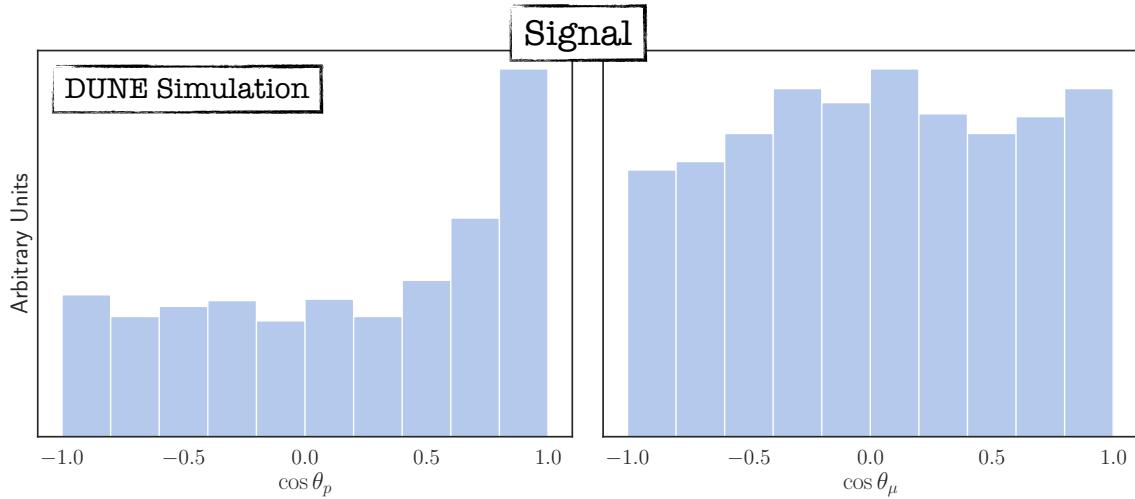
Figure 7. Signal distribution of the reconstructed proton and muon angles respect to the incoming neutrino. The proton tends to fly out forward.

We also find that a useful kinematic variable is θ_N, defined by $\cos\theta_N \equiv \hat{p}_{\odot} \cdot \vec{p}_{^{39}\mathrm{Ar}}/|\vec{p}_{^{39}\mathrm{Ar}}|$. If the neutrino does indeed arrive from the direction of the Sun with an energy of 236 MeV, then θ_N would evaluate to the angle between the reconstructed remnant nucleus momentum and the direction of the Sun. We plot a generator level (reconstruction level) 2D histogram of $\cos\theta_p$ vs. $\cos\theta_N$ in Fig. 8 (Fig. 9).

Unsurprisingly, both signal and background distributions contain events in which $\cos\theta_N$ is close to 1, since the definition of $\vec{p}_{^{39}\mathrm{Ar}}$ biases it in the forward direction. Perhaps more surprisingly, the signal distribution contains a significant population of events in which $\cos\theta_p \sim 1$, while $\cos\theta_N \sim -1$. There is no similar population of events in the background distribution, implying that a good way to reject background is to select events in which the proton is ejected in the direction away from the Sun, while $\vec{p}_{^{39}\mathrm{Ar}}$ points back to the Sun.

After reconstruction (Fig. 9), the discrimination between signal and background is poorer. Although the angular distribution for the charged lepton is isotropic, it is nevertheless correlated with that of the proton; for events where the ejected proton and recoiling nucleus are (anti-)collinear with the neutrino, the charged lepton track also lies upon the same line. In this case, the reconstruction algorithm may be unable to distinguish the proton and charged leptons tracks, leading to an event reconstructed with just a single track, which
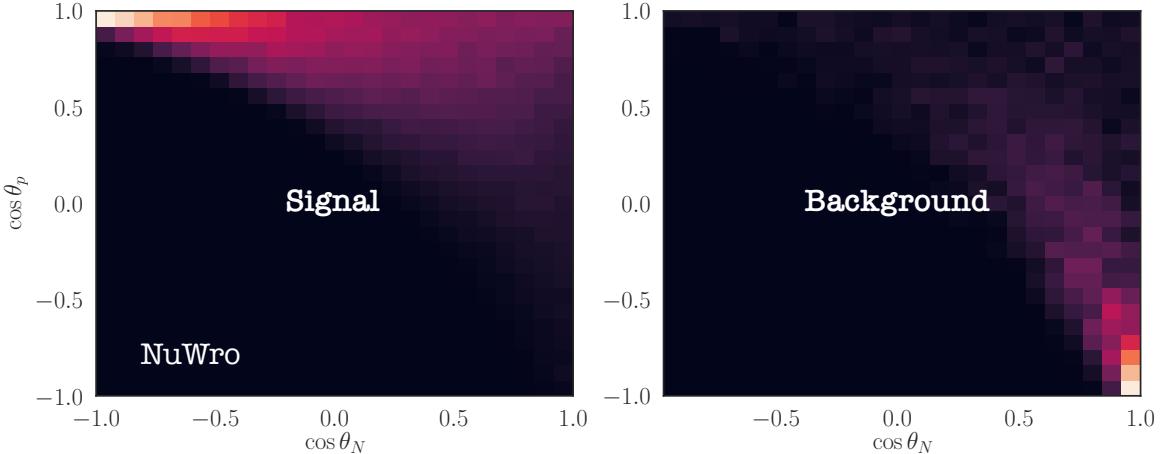
Figure 8. 2D histograms of the proton and the remnant nucleus angles respect to the incoming neutrino at the generator level (not put through the detector simulation and reconstruction). These events passed our aforementioned topology and energy selection. Note, $\cos\theta_N$ and $\cos\theta_p$ are always well-defined. Signal/background is on the left/right. For the atmospheric background, assuming that the incoming neutrino points to the Sun, rather than isotropically, violates momentum conservation and leads to an incorrect nuclear recoil and a distinct angular distribution.
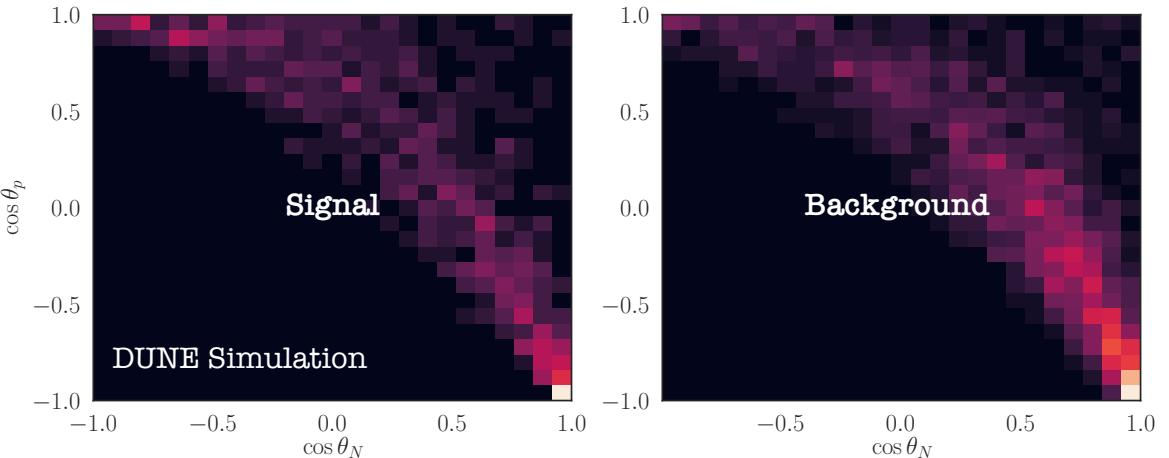
Figure 9. Reconstructed 2D histograms of $\cos\theta_p$ and $\cos\theta_N$. These events have gone through the detector simulation and reconstruction and passed the energy cut. Comparing to Fig. 8, the discrimination between the signal (left) and background (right) is much reduced due to poor reconstruction of back to back tracks.

would be rejected by the event selection cuts. However, we will see that the shift in dark matter sensitivity due to this reconstruction failure is less than $\mathcal{O}(10)$.

It may seem counterintuitive that the remnant nucleus should be backscattered in CCQE events. But an examination of the corresponding events at generator level provides an explanation; in the majority of events in which the proton is forward-directed and the remnant nucleus is backward-directed, the nucleon struck by the neutrino had an initial momentum

in the direction away from the Sun (Fig. 10). When the struck nucleon is already moving away from the Sun, the outgoing nucleon is also typically very forward-directed, while the remaining nucleons have a net momentum in the opposite direction, leading to a backward directed remnant nucleus.
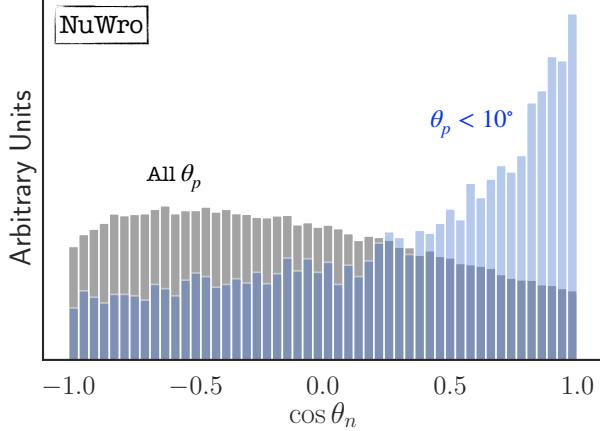

Figure 10. NuWro generated (normalized) distribution of the angles of the struck nucleons - before scattering - with respect to the incoming signal neutrino arriving from the Sun. For the grey histogram, only the event selection cuts are imposed. The blue histogram is for cases with forward ejected protons ($\theta_p < 10°$). This figure shows that such protons are correlated with nucleons which were forward-going before the interaction.
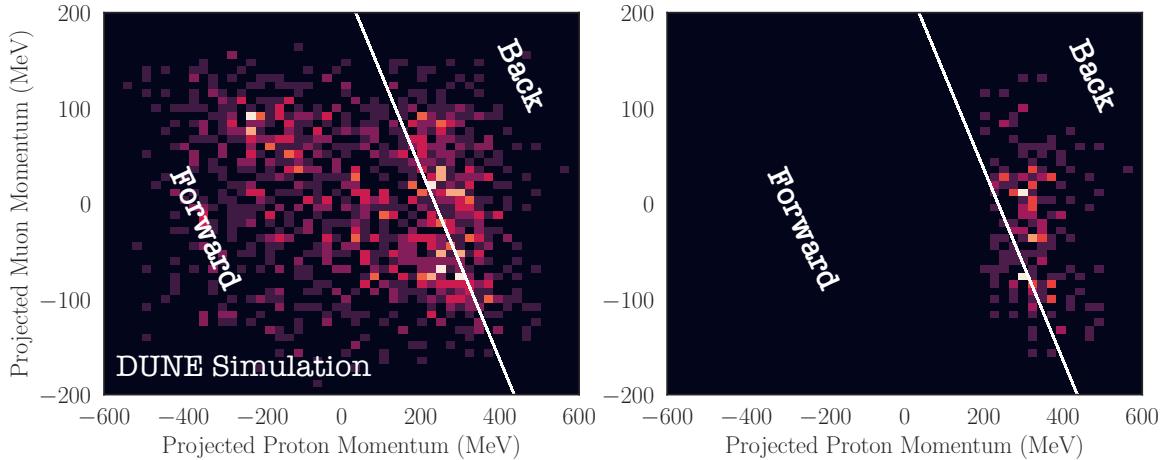
Figure 11. Signal 2D histograms of the reconstructed muon and proton momenta projected along the incoming neutrino direction. The left plot has only event selection cuts, whereas the right plot only includes such events with very forward protons ($\cos\theta_p < 30°$). The white line (($\vec{p}_\nu - \vec{p}_p - \vec{p}_\mu) \cdot \hat{p}_\nu = 0$) separates forward/backscattered remnant nuclei. Momentum conservation means that $\vec{p}_{39_{Ar}} = \vec{p}_\nu - \vec{p}_p - \vec{p}_\mu$. Hence, the nucleus backscatters when $\vec{p}_{39_{Ar}} \cdot \hat{p}_\nu < 0$ (to the right of the line). This figure emphasizes that the remnant nucleus tends to be backscattered if the proton is very forward scattered.

To illustrate this point, we plot the distribution of signal events in the $(\vec{p}_p \cdot \hat{p}_\odot, \vec{p}_\mu \cdot \hat{p}_\odot)$

plane (Figs. 11). The left panel is the distribution of all signal events passing event selection cuts, while the right panel is the distribution of such events for which $\cos\theta_p < 30°$. In both panels, the white diagonal line indicates $(\vec{p}_p + \vec{p}_\mu) \cdot \hat{p}_\odot = 236$ MeV; events to the right of this line have $\cos\theta_N < 0$, while events to the left have $\cos\theta_N > 0$,.

We define the signal efficiency η_S^μ to be the fraction of signal neutrino events which pass the event selection cuts as well as the the energy and directionality cuts we impose. Similarly, we define the background efficiency η_B^μ to be the fraction of atmospheric neutrino events with a neutrino energy between $E_{min}^{bgd} = 150$ MeV and $E_{max}^{bgd} = 400$ MeV which pass these cuts. Only a negligible fraction of atmospheric neutrinos outside the range $150 - 400$ MeV pass the cuts.

Motivated by the reconstructed energy resolution of the signal events, we impose an energy cut by selecting only events with reconstructed neutrino energy in the range 236 ± 30 MeV. Also, since protons often fly out forward, we require them to lie within an angular cone centered on the direction pointing from the Sun. A similar approach for the leptons is fruitless. At such energies, their ejection is largely isotropic. Finally, we impose cuts on $\cos\theta_N$.

Various cuts and their effect on DUNE's sensitivity to a 236 MeV flux of ν_μ emanating from the Sun are listed in Table 1.

3 Solar KDAR ν_μ Flux

We will first determine the number of background atmospheric neutrino events which are expected to pass our cuts over a given exposure of DUNE.

$$N_B^\mu = \eta_B^\mu \int_{E_{min}^{bgd}}^{E_{max}^{bgd}} dE_\nu \, d\Omega \, \frac{d^2\Phi_B^\mu}{dE_\nu d\Omega} \times \left(\bar{A}_{\text{eff}}^{(\mu)} T \right), \tag{3.1}$$

where η_B^μ, E_{min}^{bgd} and E_{max}^{bgd} are defined as in the previous section. $d^2\Phi^\mu/dE_\nu d\Omega$ is the differential flux of atmospheric ν_μ, and T is the exposure time. The effective area of DUNE effective is the product of the neutrino-nucleus scattering cross section with the number of nuclei in the fiducial volume. We take DUNE's effective area to atmospheric ν_μ, $\bar{A}_{\text{eff}}^{(\mu)}$, to be given by

$$\bar{A}_{\text{eff}}^{(\mu)} = (6.0 \times 10^{-10} \text{ m}^2) \left(\frac{\sigma_{\nu\text{-Ar}}^{(\mu)bgd.}}{10^{-38} \text{ cm}^2} \right) \left(\frac{M_{\text{target}}}{40 \text{ kT}} \right), \tag{3.2}$$

where $\sigma_{\nu\text{-Ar}}^{(\mu)bgd.}$ is the ν_μ-Ar charged-current scattering cross section, weighted by the atmospheric neutrino spectrum in the energy range $\left(E_{min}^{bgd}, E_{max}^{bgd} \right)$, as described in Section 2. Combining 3.1 and 3.2 gives

$$N_B^{(\mu)} = \eta_B^\mu (2.39) \left(\frac{\sigma_{\nu\text{-Ar}}^{(\mu)bgd.}}{10^{-38} \text{ cm}^2} \right) \left(\frac{M_{\text{target}} T}{400 \text{ kT yr}} \right) \int_{E_{min}^{bgd}}^{E_{max}^{bgd}} dE_\nu \, \frac{d^2\Phi_B^\mu}{dE_\nu d\Omega} (\text{ m}^2 \text{ s sr}). \tag{3.3}$$

Setting $E_{min}^{bgd} = 150$ MeV, $E_{max}^{bgd} = 400$ MeV, and $\sigma_{\nu\text{-Ar}}^{(\mu)bgd.} = 2.80346 \times 10^{-38}$ cm^2, we can integrate the spectrum from [19] calculated at Homestake at solar minimum, yielding

$$N_B^{(\mu)} = \eta_B^\mu \times (6.67 \times 10^3) \times (\text{exposure}/400 \text{ kT yr}). \tag{3.4}$$

Given the background acceptances η_B^μ listed in Table 1, we can then determine the number of background events expected to pass the cuts, also listed in Table 1.

We assume that the number of signal and background events seen by DUNE will be drawn from Poisson-distributions whose means are given by the expected number of signal and background events, denoted by N_S^μ and N_B^μ, respectively. To estimate the sensitivity of DUNE, we assume a representative ("Asimov" [32]) data set in which the number of observed neutrinos is taken to be the number of expected background neutrinos, rounded to the nearest integer (that is, $N_O^\mu = \text{round}(N_B^\mu)$). We denote by $N_S^{\mu,90}$ the number of expected signal events such that the likelihood of an experimental run observing a number of total events larger than $\text{round}(N_B^\mu)$ is 90%. A model for which the expected number of signal events satisfies $N_S^\mu > N_S^{\mu,90}$ lies in the region to which we estimate DUNE would be sensitive.

Given $N_S^{\mu,90}$ and η_S^μ, we can then straightforwardly determine $\Phi_{236\text{ MeV}}$, the maximum flux of 236 MeV neutrinos emanating from the core of the Sun which would be allowed (at 90% CL), given that DUNE observed only a number of events consistent with atmospheric neutrino background.

$$\Phi_{236\text{ MeV}} = \frac{N_S^{\mu,90}}{\eta_S^\mu A_{\text{eff}}^{(\mu)}(E_\nu) T} = 5.3\text{ m}^{-2}\text{ s}^{-1} \frac{N_S^\mu}{\eta_S^\mu} \left(\frac{\sigma_{\nu\text{-Ar}}^{(\mu)}(E_\nu)}{10^{-38}\text{ cm}^2} \right)^{-1} \left(\frac{\text{exposure}}{400\text{ kT yr}} \right)^{-1}, \quad (3.5)$$

where

$$A_{\text{eff}}^{(\mu)}(E_\nu) = (6.0 \times 10^{-10}\text{ m}^2) \left(\frac{\sigma_{\nu\text{-Ar}}^{(\mu)}(E_\nu)}{10^{-38}\text{ cm}^2} \right) \left(\frac{M_{\text{target}}}{40\text{ kT}} \right), \quad (3.6)$$

and $\sigma_{\nu\text{-Ar}}^{(\mu)}(E_\nu = 236\text{ MeV}) = 2.6 \times 10^{-38}\text{ cm}^2$.

$\Phi_{236\text{ MeV}}$ is our primary result, and represents the minimum flux of 236 MeV ν_μ emanating from the core of the Sun to which DUNE would be sensitive with any given exposure. This result is independent of the the specific model of new physics which generates this excess flux of neutrinos, but is determined only by the efficiency with which 236 MeV neutrinos from the core of the Sun and atmospheric background neutrinos pass the cuts.

We plot $\Phi_{236\text{ MeV}}$ in Figure 12, as a function of the exposure, for several different choices of cuts (see Table 1). In each case, the reconstructed neutrino energy is required to be in the range 236 ± 30 MeV. In one case, cuts on θ_N and θ_p are chosen to optimize signal significance (solid lines), while in the other case, these cuts are chosen to optimize the signal-to-background ratio (that is, η_S/η_B) (dashed lines). To illustrate the effect of possible improvements in track reconstruction, we also apply this analysis framework directly to the muon and proton tracks produced by the event generator; these curves are presented as green lines. All four of the angular cut choices, along with their efficiencies, sensitivities, signal-to-background ratios, and number of expected signal and background events, are listed in Table 1. For the cuts (applied to reconstructed events) which maximize the S/B, the sensitivity varies discontinuously. This is because, in this case, the number of assumed events observed is small, and the jumps are where they vary discontinuously.

3.1 Application: Search for Inelastically Scattered Dark Matter

To place this result in context, we consider a dark matter scenario which can be constrained by data from DUNE, but which would be difficult to constrain with direct detection experiments. In particular, we consider the case of low-mass dark matter ($m_X \lesssim 10$ GeV)
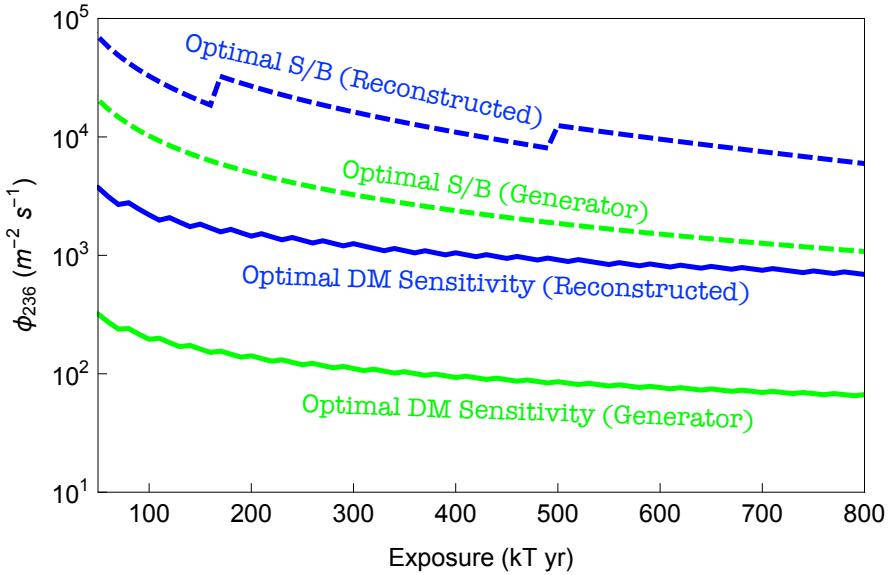
Figure 12. DUNE sensitivity to $\phi_{236\ \text{MeV}}$, the flux of 236 MeV ν_μ's from the Sun, independent of the new physics model that produces them. The blue lines correspond to the reconstructed quantities in the first and second rows of Table 1 and the green lines correspond to the generator level quantities in the third and fourth rows. The dashed lines are for maximum S/B and the filled lines are for maximum DM sensitivity. The discontinuities are due to the limit of small numbers of events; noticeable when the number of observed events jumps by one.

which scatters inelastically with nuclei, with the emerging dark particle being $\delta = 50$ keV heavier than the incoming dark matter particle. In this case, dark matter inelastic scattering is kinematically inaccessible for detectors on Earth, because there is insufficient energy to produce the excited state. But because dark matter accelerates as it approaches the Sun, it may have sufficient kinetic energy to scatter inelastically against solar nuclei, leading to its gravitational capture [23–26].

One example of a scenario in which inelastic scattering can dominate is the case in which the dark matter is charged under a spontaneously-broken $U(1)$ gauge symmetry. In this case, a dark matter vector current couples to the dark photon, which can be mediate dark matter-nucleon scattering. The tree-level scattering process is necessarily inelastic, because the vector current for a single real particle vanishes. Elastic scattering is instead subleading, mediated either by multiple dark photon exchange or by other mediators with small couplings. Although the size of this subleading elastic scattering cross section is model-dependent, it can be well below current direct detection sensitivity.

After the initial inelastic scatter, the dark matter is gravitationally captured, and continues to orbit the Sun. As the dark matter passes through the Sun many times, subsequent inelastic or elastic scatters result in an even greater loss of dark matter kinetic energy, until the particle settles in the core of the Sun [27, 28]. Once the dark matter has lost enough kinetic energy, inelastic scattering is no longer kinematically possible, but since the dark matter continues to pass through the Sun many times during the Sun's lifetime, even the subleading elastic scattering cross section can be sufficient to deplete the dark matter kinetic energy enough for it to settle in the core.

After gravitational capture, we assume dark matter annihilation to first generation

quarks, with dark matter capture and annihilation being in equilibrium. Even though dark matter annihilation produces only first-generation quarks, a substantial number of kaons are produced by subsequent fragmentation and hadronization processes. If the dark matter mass is $\gtrsim \mathcal{O}(5 \text{ GeV})$, then the center of mass energy is large compared to the kaon mass, and the up, down, and strange quarks can all be treated as light quarks.

We assume that dark matter scattering with nuclei is spin-independent and velocity-independent, with an equal coupling to protons and neutrons. Because $\delta \ll m_X$, the dark matter-nucleon scattering matrix element is largely independent of δ. The dependence of the dark matter-nucleus scattering cross section on δ arises from the final state phase space. Thus, we will parameterize the dark matter model by σ_0, which is the total cross section for dark matter-nucleon scattering, extrapolated to $\delta = 0$. From this quantity, the differential cross section for scattering against any nucleus at $\delta = 50$ keV can be determined.

In this scenario, the DM annihilation rate (Γ_A) is equal to one-half of the dark matter capture rate (Γ_C). The capture rate is directly proportional to σ_0, with $\Gamma_C = C_\delta(m_X) \times \sigma_0$. The proportionality constant $C_\delta(m_X)$ is determined entirely by the dark matter mass, by solar physics, and the assumption that dark matter has a nominal Maxwell-Boltzmann velocity distribution with a density of 0.3 GeV/ cm^3. Relevant values for the $C_\delta(m_X)$ can be found in [29].

In this scenario, we can relate $\Phi_{236 \text{ MeV}}$ to σ_0, finding

$$\Phi_{236 \text{ MeV}} = \frac{(C_\delta(m_X) \times \sigma_0/2)F^\mu}{4\pi r_\oplus^2} \left(0.64 \times \frac{2m_X}{m_K} r_K(m_X) \right),$$
$$= (3.1 \times 10^4 \text{ m}^{-2} \text{ s}^{-1}) \left(\frac{C_\delta(m_X)}{10^{29} \text{ pb}^{-1} \text{ s}^{-1}} \right) \left(\frac{\sigma_0}{\text{pb}} \right) \left(\frac{2m_X}{m_K} r_K(m_X) \right) \quad (3.7)$$

where $F^\mu = 0.27$ is the fraction of 236 MeV neutrinos which arrive at the detector as ν_μ, assuming a normal hierarchy. While an experimental data analysis requires a full treatment of neutrino oscillations to obtain neutrino spectra and flavor ratios for specific times of detector operation, for this analysis it is sufficient to assume an annual averaged flavor ratio taken from [9] (if one assumed an inverted hierarchy F^μ would increase by at most 25%). $r_\oplus = 1.5 \times 10^{11}$ m is the distance from the Sun to the Earth, and $r_K(m_X)$ is the fraction of the center of mass energy of the dark matter initial state which is converted into stopped K^+ through dark matter annihilation, the hadronization and fragmentation of the outgoing particles, and the interactions of those particles with the dense solar medium (values for $r_K(m_X)$ can be found in [8]). The factor 0.64 is the branching fraction for K^+ decay to produce a monoenergetic 236 MeVν_μ. We can thus relate $\Phi_{236 \text{ MeV}}$ to a 90% CL exclusion contour in the (m_X, σ_0)-plane.

In Figure 13, we plot the 90% CL sensitivity of DUNE (400 kT yr) in the (m_X, σ_0)-plane for the case where WIMPs annihilate solely to first generation quarks, assuming a search for monoenergetic neutrinos at 236 MeV from stopped K^+ decay. We plot sensitivity curves for each of the four cuts strategies given in Table 1.

There are a variety of other theoretical uncertainties which can have a significant effect on DUNE's sensitivity. For example, we have assumed that dark matter annihilates to first generation quarks. If dark matter annihilates instead to second generation quarks, the average number of K^+ produced per annihilation (and, thus, the flux of 236 MeV neutrinos) would increase by about a factor of 2. Furthermore, we have modeled neutrino-nucleus scattering at this energy with NuWro. Although there are experimental measurements of this
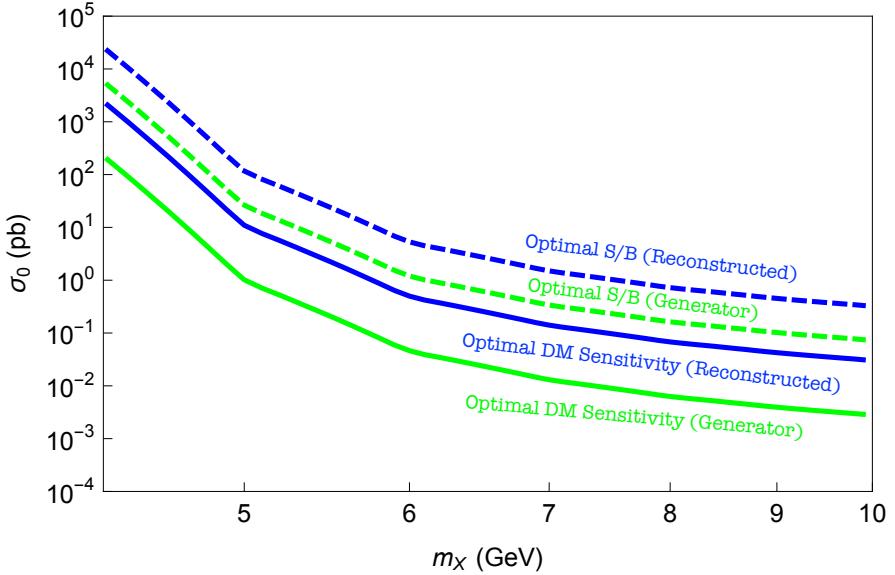
Figure 13. Projected 90% sensitivity curves for DUNE (400 kT yr) for inelastic dark matter scattering. All the curves are for the stopped K^+ channel. The relevant cuts are listed in Fig. 12 and Table 1.

Table 1. The angular cuts (including the energy cut of 236 ± 30 MeV) and the resulting signal and background efficiencies, the expected number of signal and background events, the expected signal to background ratio at DUNE, and the maximum flux of 236 MeV neutrinos emanating from the Sun which would be allowed (at 90% CL). The first two rows are cuts on reconstructed events and the last two rows are cuts on generator level events (no detector simulation/reconstruction). We include the generator level information to illustrate the optimistic case of perfect reconstruction.

$\theta_P^{reco} <$	$\theta_N^{reco} >$	η_S^{reco}	η_B^{reco}	$N_S^{reco,90}$	N_B^{reco}	S/B^{reco}	$\Phi_{236\ \text{MeV}}^{reco}[\text{ m}^{-2}\text{ s}^{-1}]$
$60°$	$162°$	5.0×10^{-4}	1.9×10^{-4}	2.7	1.2	2.2	1.1×10^4
$60°$	$60°$	2.7×10^{-2}	1.4×10^{-2}	13.9	92.7	0.2	1.1×10^3
$\theta_P <$	$\theta_N >$	η_S	η_B	N_S^{90}	N_B	S/B	$\Phi_{236\ \text{MeV}}[\text{ m}^{-2}\text{ s}^{-1}]$
$50°$	$171°$	1.8×10^{-3}	3.3×10^{-5}	2.1	0.2	10.5	2.4×10^3
$50°$	$20°$	3.9×10^{-1}	2.6×10^{-2}	17.8	173.3	0.1	93.1

cross section, there are still significant uncertainties, both in the magnitude of the charged-current cross section and in the angular dependence. But any stopped pion experiment also acts as a stopped kaon experiment [30], and a variety of future KDAR measurements are under consideration [31], and would serve as a calibration for this type of analysis. Importantly, DUNE itself can provide calibration data, by searching off-axis.

Future improvements in reconstruction techniques that could enable electron channel to be used effectively, would lead to a significant improvement in sensitivity. The electron channel is generally expected to be more sensitive than the muon channel for three reasons [10]. First, the atmospheric neutrino background flux is smaller. Second, the effective area of DUNE is larger for 236 MeV ν_e than for ν_μ, because the charged-current scattering

cross section for ν_μ is suppressed by the reduced phase space of the outgoing muon. Third, the flux of 236 MeV ν_e arriving at Earth from KDAR in the Sun is expected to be larger than the flux of 236 MeV ν_μ as a result of oscillation effects in the dense medium of the Sun (assuming a normal hierarchy) [9].

4   Conclusion

In this work, we have estimated DUNE's potential to detect the monoenergetic 236 MeV neutrinos arising from kaon-decay-at-rest in the core of the Sun. Although the charged leptons produced from a charged-current interaction of a 236 MeV neutrino are roughly isotropic, many such interactions produce an ejected proton which is forward-directed. Moreover, the remnant nucleus tends to be backward-directed, and observable kinematic variables can be used as a proxy for the remnant nucleus momentum, allowing for better discrimination of signal from background.

We have used these observables in a realistic manner, with the response of the detector modelled numerically. Although we have found that the discrimination of signal from background, S/B, can be as large as 2.2 for a model where there are enough signal events to exclude, a realistic treatment of the detector results in reduced sensitivity with respect to earlier estimates.

Foreseeing future improvements in reconstruction (for example, via machine learning), we calculated the expected number of signal and background events which pass our cuts at the generator level (see Table 1). We've also plotted the generator level dark matter sensitivity curves in green in Fig. 12. These are the limits in the optimistic case of perfect reconstruction, and we find that this optimal sensitivity matches estimates made previously [10].

There are a variety of non-standard scenarios for dark matter particle physics and astrophysics in which the sensitivity of direct detection experiments is suppressed, and the flux of 236 MeV neutrinos produced in the Sun's core may provide an excellent indirect probe of dark matter interactions. In this case, DUNE's ability to identify 236 MeV neutrinos arriving from the direction of the Sun, while rejecting background, can provide unique control over systematic uncertainties. As an example, we have estimated DUNE's sensitivity to low-mass dark matter which scatters inelastically, with a mass splitting of $\delta = 50$ keV. This is an example of a dark matter process which is kinematically inaccessible for direct detection experiments on Earth, but for which a search for neutrinos at DUNE may lead to a discovery.

The search for direct evidence of non-gravitational interactions between dark matter and Standard Model matter has thus far yielded no conclusive positive signals. This has led to broader theoretical and experimental approaches to dark matter searches, and KDAR neutrinos can play an important role. It would be interesting to further study the theoretical scenarios in which searches for KDAR neutrinos provide a competitive advantage.

On the experimental side, it would also be interesting to study in more detail how the particle identification and track reconstruction at DUNE could be improved in the energy range relevant for KDAR searches. A possible DUNE module-of-opportunity may use a wireless design with an isotropic response and could improve the sensitivity to dark matter annihilation in the Sun, by reducing the loss of efficiency associated with the orientation of the Sun with respect to the DUNE wires.

Acknowledgments

References

[1] J. Spitz, Phys. Rev. D **89**, no. 7, 073007 (2014) [arXiv:1402.2284 [physics.ins-det]].

[2] A. A. Aguilar-Arevalo *et al.* [MiniBooNE Collaboration], Phys. Rev. Lett. **120**, no. 14, 141802 (2018) doi:10.1103/PhysRevLett.120.141802 [arXiv:1801.03848 [hep-ex]].

[3] J. Silk, K. A. Olive and M. Srednicki, Phys. Rev. Lett. **55**, 257 (1985).

[4] W. H. Press and D. N. Spergel, Astrophys. J. **296**, 679 (1985).

[5] L. M. Krauss, K. Freese, W. Press and D. Spergel, Astrophys. J. **299**, 1001 (1985).

[6] C. Rott, J. Siegal-Gaskins and J. F. Beacom, Phys. Rev. D **88**, 055005 (2013) [arXiv:1208.0827 [astro-ph.HE]].

[7] N. Bernal, J. Martín-Albo and S. Palomares-Ruiz, JCAP **1308**, 011 (2013) [arXiv:1208.0834 [hep-ph]].

[8] C. Rott, S. In, J. Kumar and D. Yaylali, JCAP **1511**, no. 11, 039 (2015) [arXiv:1510.00170 [hep-ph]].

[9] R. Lehnert and T. J. Weiler, Phys. Rev. D **77**, 125004 (2008) [arXiv:0708.1035 [hep-ph]].

[10] C. Rott, S. In, J. Kumar and D. Yaylali, JCAP **1701**, 016 (2017) doi:10.1088/1475-7516/2017/01/016 [arXiv:1609.04876 [hep-ph]].

[11] C. Rott, S. In, J. Kumar and D. Yaylali, arXiv:1710.03822 [hep-ph].

[12] R. Acciarri *et al.* [DUNE Collaboration], arXiv:1512.06148 [physics.ins-det].

[13] B. Abi *et al.* [DUNE Collaboration], JINST **15**, P12004 (2020) doi:10.1088/1748-0221/15/12/P12004 [arXiv:2007.06722 [physics.ins-det]].

[14] E. Church [LArSoft Collaboration] [arXiv:1311.6774 [physics.ins-det]].

[15] J. Allison *et al.*, IEEE Trans. Nucl. Sci. **53**, no. 1 (2006) 270-278 doi:10.1109/TNS.2006.869826

[16] J. S. Marshall and M. A. Anderson, Eur. Phys. J **C75**, no. 9 (2015) 439 doi:10.1140/epjc/s10052-015-3659-3 [arXiv:1506.05348 [physics.data-an]].

[17] L. I. Ponomarev, Ann. Rev. Nucl. Part. Sci. **23**, 395 (1973).

[18] T. Golan, J. T. Sobczyk and J. Zmuda, Nucl. Phys. Proc. Suppl. **229-232**, 499 (2012). doi:10.1016/j.nuclphysbps.2012.09.136

[19] http://www.icrr.u-tokyo.ac.jp/ mhonda/

[20] A. M. Ankowski and J. T. Sobczyk, AIP Conf. Proc. **967**, 106 (2007) [arXiv:0709.2139 [nucl-th]].

[21] T. Golan, C. Juszczak and J. T. Sobczyk, Phys. Rev. C **86**, 015505 (2012) [arXiv:1202.4197 [nucl-th]].

[22] C. Rott, D. Jeong, J. Kumar and D. Yaylali, JCAP **1907**, 006 (2019) doi:10.1088/1475-7516/2019/07/006 [arXiv:1903.04175 [astro-ph.HE]].

[23] A. Gould, Astrophys. J. **321**, 571 (1987).

[24] A. Gould, Astrophys. J. **388**, 338 (1992).

[25] R. Garani and S. Palomares-Ruiz, JCAP **05**, 007 (2017) doi:10.1088/1475-7516/2017/05/007 [arXiv:1702.02768 [hep-ph]].

[26] A. Nuñez-Castiñeyra, E. Nezri and V. Bertin, JCAP **12**, 043 (2019) doi:10.1088/1475-7516/2019/12/043 [arXiv:1906.11674 [astro-ph.GA]].

[27] S. Nussinov, L. T. Wang and I. Yavin, JCAP **08**, 037 (2009) doi:10.1088/1475-7516/2009/08/037 [arXiv:0905.1333 [hep-ph]].

[28] A. Menon, R. Morris, A. Pierce and N. Weiner, Phys. Rev. D **82**, 015011 (2010) doi:10.1103/PhysRevD.82.015011 [arXiv:0905.1847 [hep-ph]].

[29] J. Kumar, J. G. Learned, S. Smith and K. Richardson, Phys. Rev. D **86**, 073002 (2012) [arXiv:1204.5120 [hep-ph]].

[30] J. Spitz, Phys. Rev. D **85**, 093020 (2012) [arXiv:1203.6050 [hep-ph]].

[31] J. M. Conrad, Nucl. Phys. Proc. Suppl. **229-232**, 386 (2012) [arXiv:1012.4853 [hep-ex]].

[32] G. Cowan, K. Cranmer, E. Gross *et al.*, Eur. Phys. J C**71**, 1554 (2011) doi:10.1140/epjc/s10052-011-1554-0